Cell Reports

Article

Fatty acids impact sarcomere integrity through myristoylation and ER homeostasis

Graphical abstract

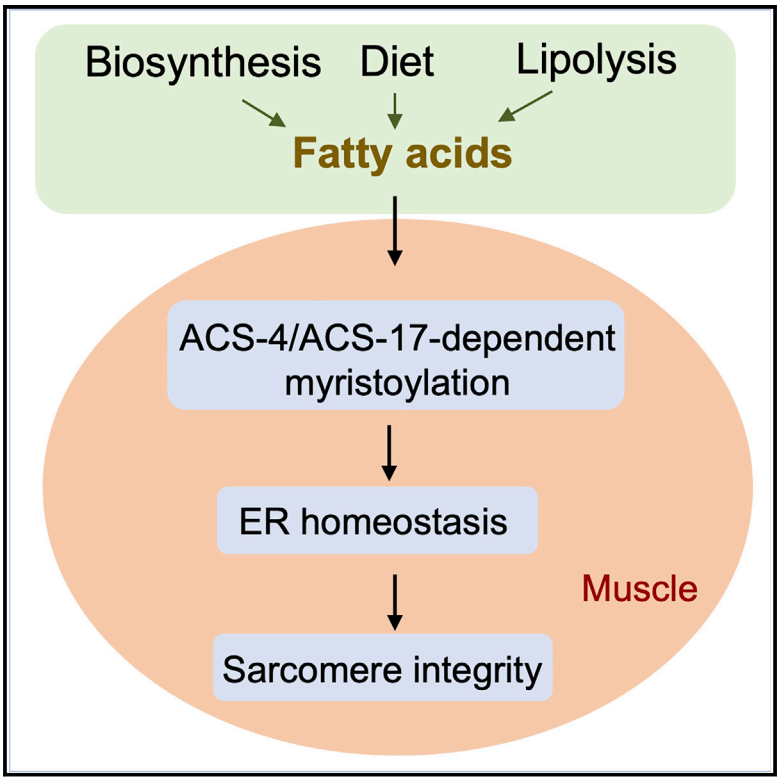

Authors

Hongyun Tang, Mingxue Cui, Min Han

Correspondence

mhan@colorado.edu

In brief

Tang et al. show that fatty acid deficiency causes defects in muscle integrity in the nematode *C. elegans* and such an impact is mediated by deficiency of lipid modification of specific proteins in the muscle that in turn triggers ER stress and muscle disorganization. The results reveal the regulatory roles of fatty acids and ER homeostasis in muscle maintenance.

Highlights

- Disrupting FA biosynthesis causes muscle defects and paralysis in *C. elegans*
- Blocking protein myristoylation results in muscle defects and paralysis in *C. elegans*
- ER stress and UPR^{ER} in muscle play key roles in mediating the impacts
- Reduction of sarcomere component PINCH is a critical downstream event

Tang et al., 2021, Cell Reports *36*, 109539
August 17, 2021
https://doi.org/10.1016/j.celrep.2021.109539

CellPress

Cell Reports

CellPress
OPEN ACCESS

Article

Fatty acids impact sarcomere integrity through myristoylation and ER homeostasis

Hongyun Tang,[1,2,3,4] Mingxue Cui,[1,4] and Min Han[1,5,*]
[1]Department of MCDB, University of Colorado Boulder, Boulder, CO 80309, USA
[2]Key Laboratory of Growth Regulation and Transformation Research of Zhejiang Province, School of Life Sciences, Westlake University, Hangzhou 310024, Zhejiang Province, China
[3]Institute of Biology, Westlake Institute for Advanced Study, 18 Shilongshan Road, Hangzhou 310024, Zhejiang Province, China
[4]These authors contributed equally
[5]Lead contact
*Correspondence: mhan@colorado.edu
https://doi.org/10.1016/j.celrep.2021.109539

SUMMARY

Decreased ability to maintain tissue integrity is critically involved in aging and degenerative diseases. Fatty acid (FA) metabolism has a profound impact on animal development and tissue maintenance, but our understanding of the underlying mechanisms is limited. We investigated whether and how FA abundance affects muscle integrity using *Caenorhabditis elegans*. We show that reducing the overall FA level by blocking FA biosynthesis or inhibiting protein myristoylation leads to disorganization of sarcomere structure and adult-onset paralysis. Further analysis indicates that myristoylation of two ARF guanosine triphosphatases (GTPases) critically mediates the effect of FA deficiency on sarcomere integrity through inducing endoplasmic reticulum (ER) stress and ER unfolded protein response (UPR^{ER}), which in turn leads to reduction of the level of sarcomere component PINCH and myosin disorganization. We thus present a mechanism that links FA signal, protein myristoylation, and ER homeostasis with muscle integrity, which provides valuable insights into the regulatory role of nutrients and ER homeostasis in muscle maintenance.

INTRODUCTION

Fatty acids (FAs) are essential molecules in many fundamental cellular functions (e.g., energy production and membrane formation). Animals have developed mechanisms that sense the level of FAs to adapt to fluctuating nutrient conditions through regulating cellular and developmental programs. For example, fat deficiency has been known to limit female reproductive development and cause muscle loss to improve starvation survival (Lipina and Hundal, 2017; Reznick and Braun, 1987; Tang and Han, 2017). In addition, abnormal FA metabolism has been linked to certain muscular diseases (Laforêt and Vianey-Saban, 2010; Lipina and Hundal, 2017; Saini-Chohan et al., 2012). However, the mechanisms by which FAs affect muscle integrity, and the potential role of lipid-sensing systems in these processes, remain to be investigated. Understanding the molecular basis underlying the role of FAs in muscle maintenance will provide valuable insights into the pathogenesis of muscle-degenerative diseases and potential therapeutic approaches (Rüegg and Glass, 2011; Tabebordbar et al., 2013).

The highly conserved endoplasmic reticulum (ER) unfolded protein response (UPR^{ER}) regulatory pathway is an important part of the cellular stress response network that maintains cellular proteostasis and health in response to unfavorable changes in environment and cellular activities, including nutrient status (D'Amico et al., 2017; Kim et al., 2016; Labbadia and Morimoto, 2015; Walter and Ron, 2011; Wang and Kaufman, 2016). However, during prolonged ER stress, the UPR^{ER} machinery may switch from promoting cellular protection to causing cellular injury, which contributes to various pathologies, including neurodegeneration, inflammation, diabetes, and aging (Frakes and Dillin, 2017; Hetz and Saxena, 2017; Martínez et al., 2017; Wang and Kaufman, 2016). The physiological consequences of ER stress differ drastically depending on the physiological context, suggesting that molecular changes in UPR^{ER} caused by different stressors vary under different physiological conditions (Hetz and Saxena, 2017; Wang and Kaufman, 2016). Recent studies also suggested that the UPR^{ER} plays a significant role in myogenesis and muscle regeneration (Bohnert et al., 2018). However, the mechanisms underlying this role and the connection of this role to lipid metabolism remain to be explored. Elucidating whether and how FAs affect muscle integrity through modulating ER proteostasis may shed light on the pathogenesis of degenerative diseases caused by poor nutrient conditions and metabolic disorders.

Caenorhabditis elegans is an excellent model system to study muscle function, development, and organization, as the sarcomere proteins and structure are conserved between *C. elegans* and mammals, and the work regarding sarcomere assembly in *C. elegans* has advanced the understanding of adhesion complexes in mammals (Gieseler et al., 2017; Labouesse and Georges-Labouesse, 2003; Moerman and Williams, 2006;

Moerman and Fire, 1997; Waterston, 1988; Wehrle-Haller and Imhof, 2002). Our previous work demonstrated that protein myristoylation responds to the change in FA levels to modulate sex determination and oogenesis, which points to a mechanism of reproductive adaptation to nutrient deprivation (Tang and Han, 2017). In this study, we investigated the mechanism by which FA signals regulate the maintenance of muscle integrity, with the focus on the roles of protein myristoylation and ER homeostasis.

RESULTS

Deficiency in overall FA biosynthesis or protein myristoylation in muscle causes defects in myosin organization and animal mobility

To investigate the role of FA levels in the maintenance of muscle integrity, we tested whether a low cellular FA level would cause changes in the organization of myosin, a key component of the sarcomere (Moerman and Williams, 2006), in the body-wall muscle (striated muscle) of *C. elegans*. We observed that knocking down FA biosynthesis genes *fasn-1* (Lee et al., 2010) or *pod-2* (Rappleye et al., 2003) resulted in disruption of the proper organization of myosin into assembled thick filaments (A bands) in about 1/3 of animals carrying the *myo-3::*GFP extrachromosomal array (Figures 1A–1D and 1I). Animals with disorganized myosin also showed mobility defects, including uncoordinated movement and paralysis (Figure 1J).

Our previous study showed that protein myristoylation responded to changes in the cellular FA level (Tang and Han, 2017), so we probed the role of myristoylation in myosin organization. We found that muscle-specific RNAi against *nmt-1*, encoding an N-myristoyl transferase (Galvin et al., 2014), caused disorganized myosin and mobility defects in about 1/4 of the animals (Figures 1E, 1F, 1I, and 1J). *nmt-1* is an essential gene (Galvin et al., 2014), and the low penetrance of the phenotype may be due to partial reduction of the gene expression by RNAi. These results suggest that myristoylation in the body-wall muscle cells at least partially mediates the impact of FA levels on myosin organization.

Next, we analyzed the role of two acyl-coenzyme A (CoA) synthetase genes, *acs-4* and *acs-17* (Figure 1A). These two enzymes function redundantly to activate free FAs for protein myristoylation in somatic tissues, as *acs-4(lf-loss of function); acs-17(lf)* double mutants exhibit severe deficiency of protein myristoylation (Tang and Han, 2017). Although the double homozygous progeny from *acs-4(lf);acs-17(lf)* mothers are embryonic lethal (Tang and Han, 2017), *acs-4(lf);acs-17(lf)* progeny from an *acs-4(lf/+);acs-17(lf)* mother are viable. We focused our analysis on these viable homozygous progenies. We observed that 100% of these viable *acs-4(lf);acs-17(lf)* mutants displayed disorganized myosin in a subset of muscle cells and paralysis at day 1 of adulthood (Figures 1G–1I and 1K). Subsequent analyses of staged animals showed that these viable *acs-4(lf);acs-17(lf)* progeny displayed normal mobility during early larval stages, but they all displayed uncoordinated movement (Unc) at the fourth larval stage (L4) and paralysis as day 1 adults (Figure S1A). Further tissue-specific rescue analyses indicated that ACS-4 expression in body-wall muscle is sufficient to support mobility (Figures 1K and S1B). Therefore, these data suggest that myristoylation in body-wall muscle impacts mobility by affecting myosin organization at late development stages.

In addition, we obtained strain KAG420, in which the MYO-3 protein was tagged with GFP at its N terminus using the CRISPR-Cas9 approach (Mergoud Dit Lamarche et al., 2018). With a single copy of the reporter transgene, this new strain displays endogenous *myo-3* gene expression and shows normal myosin filament organization up until day 13 as adults (Mergoud Dit Lamarche et al., 2018). We thus re-evaluated MYO-3::GFP expression with this transgene in *acs-4(lf);acs-17(lf)* double mutants and obtained similar results in day 1 adults as previously observed using the extrachromosomal MYO-3::GFP transgene (Figures S1C and S1D). We also analyzed older adult animals and observed severe fragmentation of thick myosin filaments and aggregated MYO-3::GFP clumps in all body-wall muscle cells of day 4 adult *acs-4(lf);acs-17(lf)* double mutants (Figures S1E–S1H). Interestingly, we noticed that those body-wall muscle cells in the mid-body displayed more severe disorganized myosin than those body-wall muscle cells at either end in day 1 adults (Figures S1C and S1D), which may explain why *acs-4(lf);acs-17(lf)* adult animals were paralyzed in a curly shape and bent at the mid-body (Figure S1J). In day 4 *acs-4(lf);acs-17(lf)* adult animals, all body-wall muscle cells, including those at either end, showed severe myosin disorganization (Figures S1E–S1I).

Protein myristoylation affects UNC-97/PINCH level to control sarcomere integrity

To determine how *acs-4* and *acs-17* impact myosin organization, the expression and localization of actin thin filaments, as well as several components of integrin adhesion complexes (UNC-97(PINCH), PAT-3(beta-integrin), PAT-6(alpha-parvin), and UNC-112(kindlin)), were examined using GFP fusion proteins (Figures 2A–2D and S2A–S2H). Integrin adhesion complexes lie at the base of M lines and dense bodies and at adhesion plaques of the muscle cell boundaries (Rogalski et al., 2000; Lin et al., 2003). In *C. elegans*, UNC-97(PINCH) interacts with several proteins that directly or indirectly interact with MYO-3(myosin) (Qadota et al., 2007). We observed that the expression of PINCH/UNC-97::GFP from an integrated transgene (Hobert et al., 1999) was drastically decreased in both the cytoplasm and nuclei for a subset of body-wall muscle cells in day 1 adult *acs-4(lf);acs-17(lf)* double mutants when compared to either *acs-4(lf/+);acs-17(lf)* or wild-type control animals (Figures 2A–2C and S2K–S2R). UNC-97::GFP localization in both sarcomere and nuclei was significantly affected and presented in clumps (Figures 2A–2C and S2K–S2R). Western blot analysis also indicated that the UNC-97::GFP level from the whole *acs-4(lf);acs-17(lf)* worm was decreased and this reduction started at L4 stage (Figures 2D, S2A, and S2B), when the *acs-4(lf);acs-17(lf)* double mutants began to show the mobility defect (Figure S1A). Intriguingly, the UNC-97::GFP protein level in the *acs-4(lf);acs-17(lf)* double mutants was significantly higher than that in the *acs-4(lf/+);acs-17(lf)* control at L2 and L3 stages (Figures S2A and S2B), implicating a very different response of UNC-97 transgene to the myristoylation defect at early larval stages.

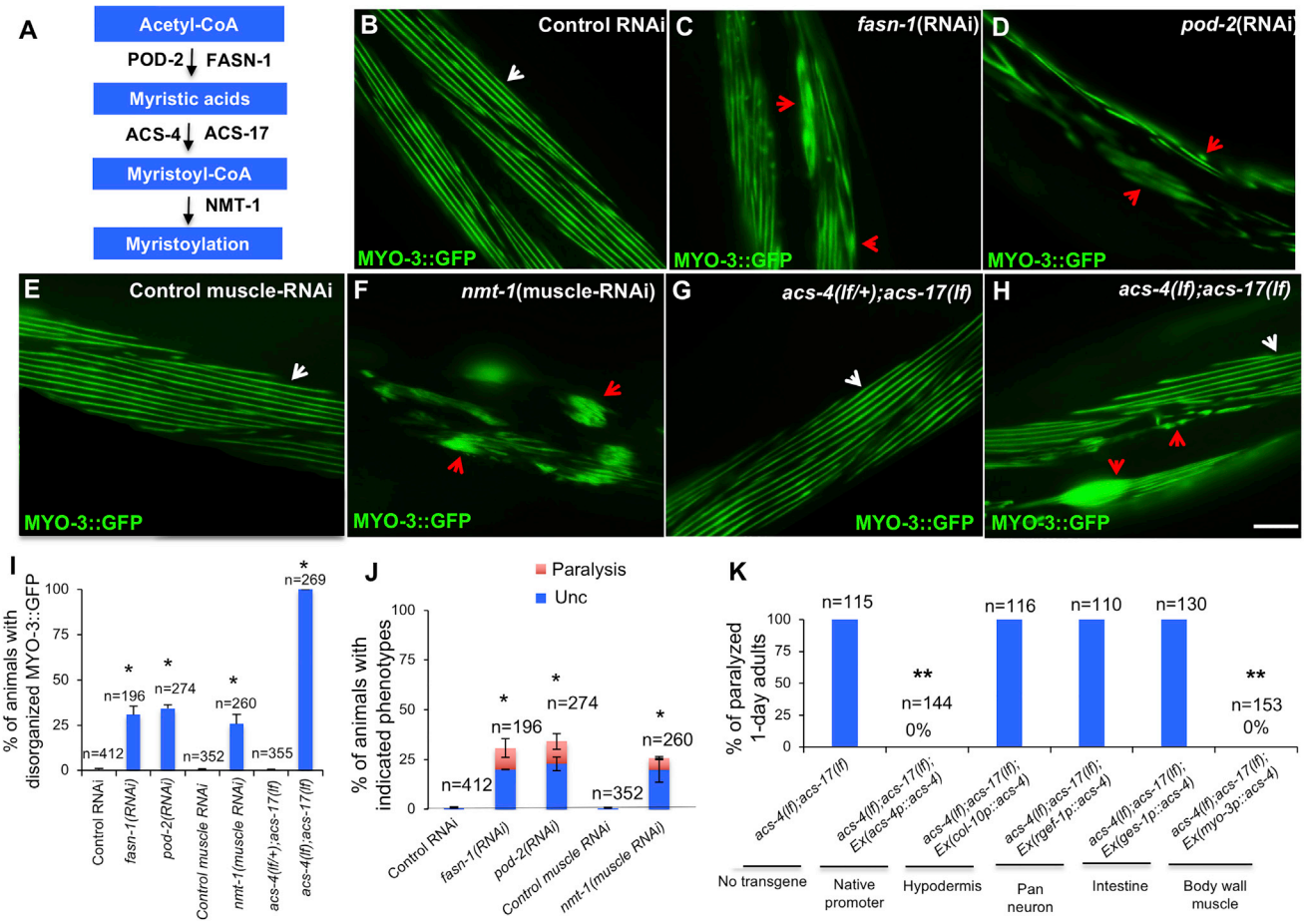

Figure 1. Fatty acid synthesis and protein myristoylation impact worm mobility and myosin organization

(A) Cartoon diagram to indicate the roles of genes involved in the tests.

(B–I) GFP images and bar graph showing that reduction of FA biosynthesis and protein myristoylation affect myosin organization. *myo-3* encodes myosin heavy chain A, and *Ex(myo-3p::MYO-3::GFP)* transgene encodes functional MYO-3::GFP (Campagnola et al., 2002). White arrows mark the organized myosin, and red arrows mark clumped myosin that indicates disorganization of sarcomeres. *lf*, loss-of-function mutation. Stage of scoring: for RNAi-treated animals in (B)–(F) and elsewhere, animals were scored 72 h post-hatch after two generations of RNAi treatment; for *acs-4(lf);acs-17(lf)* mutants in (G) and (H) and elsewhere, day 1 animals were scored (STAR Methods). Lethal animals were excluded for scoring. Bar graph (I) shows quantification of the phenotypes indicated in (B)–(H). Error bars, standard deviation. *$p < 0.05$. Scale bar, 20 μm.

(J) Bar graph indicating that FAs biosynthesis and protein myristoylation impact mobility of *C. elegans* with indicated treatment. Paralysis indicates animals with pharynx pumping but no movement; "Unc" describes worms with uncoordinated movement. Error bars, standard deviation. *$p < 0.05$.

(K) Bar graph indicating that *acs-4* functions autonomously in body-wall muscle to suppress paralysis. The robust paralysis phenotype in *acs-4(lf);acs-17(lf)* double mutants (also see Figure S1A) was suppressed by *acs-4* expression from its native promoter or body-wall-muscle-specific promoter, but not by three other tissue-specific promoters. Error bars, standard deviation. **$p < 0.005$.

Because UNC-97 is present in a complex with several other proteins, such as PAT-3, PAT-4, and PAT-6, we investigated the protein levels with GFP fusion strains and antibodies against PAT-4 and PAT-6. Our observations of the GFP fluorescence intensities suggest that the localization of PAT-3, PAT-6, and UNC-112 to M line and dense bodies was disrupted, but their expression levels were unchanged in the *acs-4(lf);acs-17(lf)* double mutants (Figures S2E–S2H). Western blot analysis also confirmed that the expression levels of PAT-6 and PAT-4 have no change in the *acs-4(lf);acs-17(lf)* double mutants (Figures S2S and S2T).

Previous studies have reported that reduction of *unc-97* results in locomotion defects ranging from slow movement to paralysis (Hobert et al., 1999; Shephard et al., 2011). Our results also indicated that muscle-specific knockdown of *unc-97* caused the paralysis, Unc, and disorganized myosin phenotypes (Figures 2E–2H) that were also observed in the *acs-4(lf);acs-17(lf)* double mutants (Figure 1). In addition, three other sarcomere components also showed disorganization in *acs-4(lf);acs-17(lf)* double mutants (Figures S2C–S2H), which were similar to reported changes in the *unc-97(lf)* mutant (Norman et al., 2007), consistent with the idea that reduction of UNC-97 contributes to the adult-onset paralysis in the *acs-4(lf);acs-17(lf)* double mutants. Furthermore, we constructed a multi-copy transgene overexpressing *unc-97* and observed suppression of the paralysis and the myosin disorganization

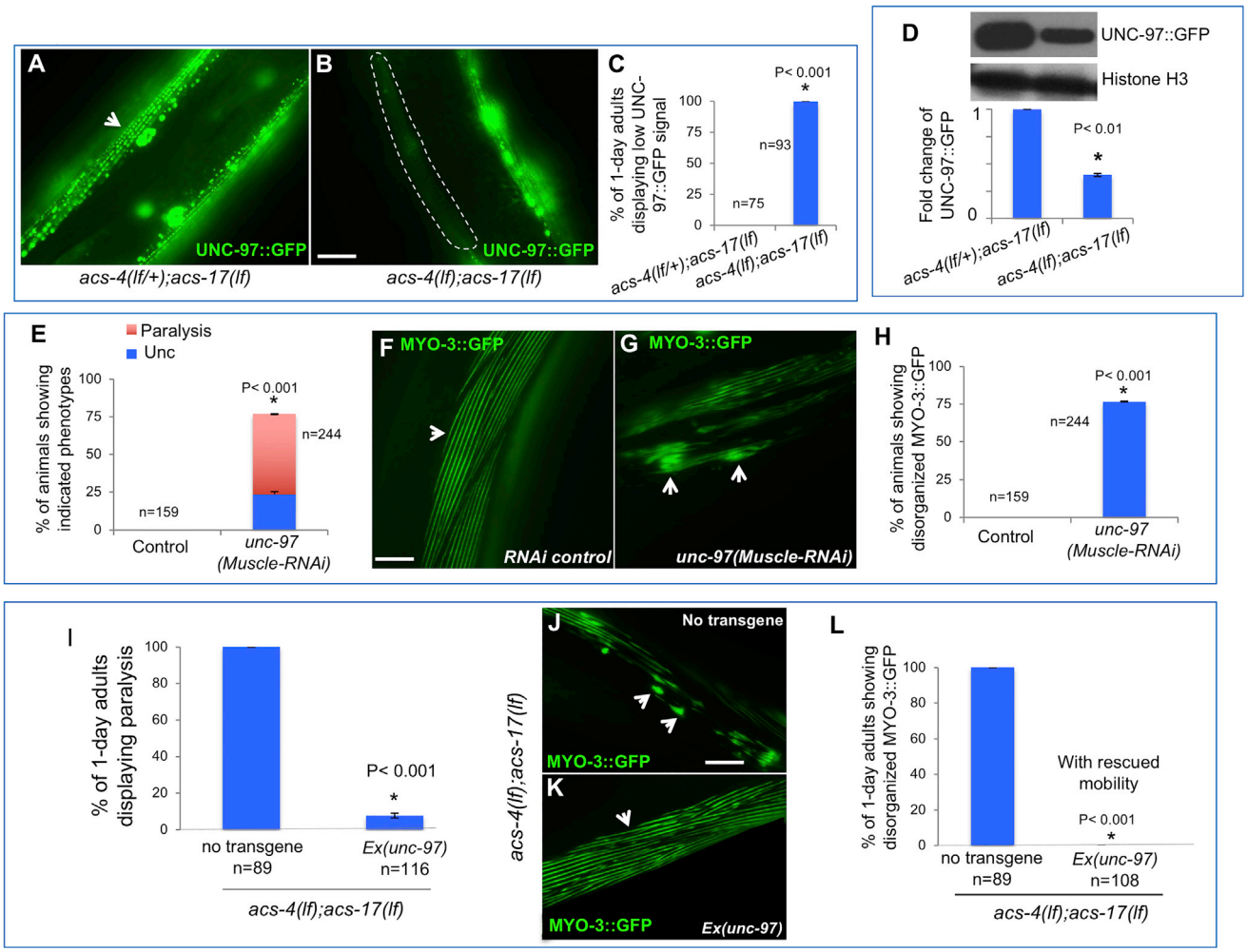

Figure 2. ACS-4 and ACS-17 regulate UNC-97/PINCH level to affect sarcomere integrity

(A–C) GFP images and bar graph showing that UNC-97/PINCH level, indicated by an UNC-97::GFP reporter expressed from an integrated transgene (mgIs25), was deceased in some muscle cells in the *acs-4(lf);acs-17(lf)* double mutants. Dashed line outlines the muscle cell displaying low UNC-97::GFP signal. Animals with obvious low GFP signal in muscle cell were scored as positive.

(D) Western blot and bar graph showing the difference of UNC-97::GFP level in whole worm protein extracts from animals with indicated genotypes. Histone H3 served as an internal control. Three biological replicates (n = 3) were performed and used for quantifications of the signals and are shown as means ± standard deviation.

(E–H) Bar graph and GFP images indicating that knocking down *unc-97* specifically in the body-wall muscle cells caused mobility and myosin organization defects. Arrows indicate organized (F) or clumped (G) myosin.

(I–L) Bar graph and GFP images showing that overexpression of *unc-97* by transgene Ex(*unc-97*) suppressed mobility and myosin organization defects in the *acs-4(lf);acs-17(lf)* animals.

(A, B, F, G, J, and K) Scale bars, 20 μm.

(C–E, H, I, and L) Error bars, standard deviation.

phenotypes at day 1 adulthood (Figures 2I–2L), although paralysis was suppressed for only 1 day. Additionally, we observed that knocking down genes in FA biosynthesis (*fasn-1* and *pod-2*) or myristoylation (*nmt-1*) also resulted in reduction of UNC-97::GFP level (Figures S2I and S2J). Together, these results indicate that decreased UNC-97 in *acs-4(lf);acs-17(lf)* double mutants contributes, at least in part, to the paralysis phenotype and that FA biosynthesis and myristoylation affect sarcomere integrity and mobility partially through affecting UNC-97 level.

Myristoylation of ARF-1.2 and ARF-3 is critically involved in the regulation of sarcomere integrity maintenance by FA level

To elucidate what myristoylated proteins are involved in the mobility defects in *acs-4(lf);acs-17(lf)* double mutants, we established a biochemical procedure (Figure S3A) and identified 40 proteins that are likely to be myristoylated in *C. elegans* (Table S1). We then performed RNAi analysis to examine the potential role of these proteins in animal mobility and observed mobility defects caused by RNAi against *arf-1.2* and *arf-3* (Table S2),

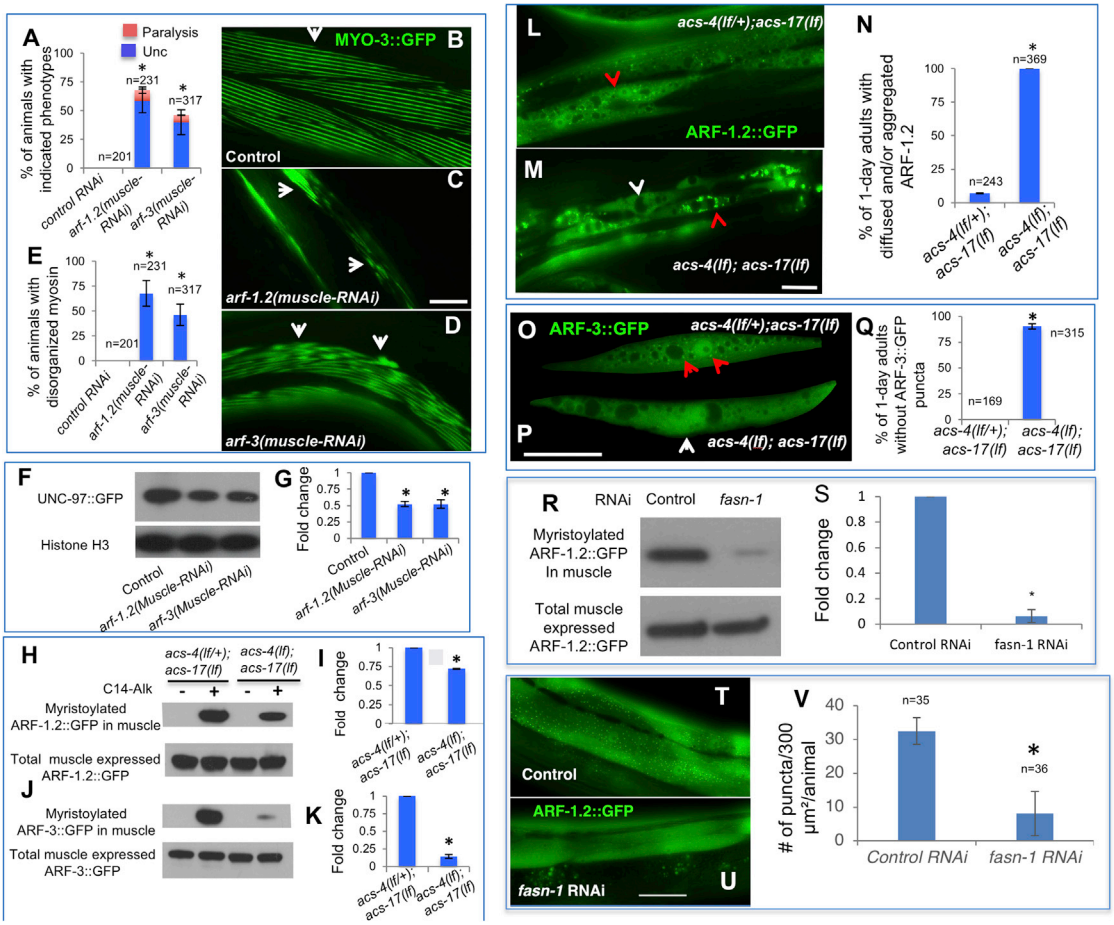

Figure 3. ACS-4 and ACS-17 modulate myristoylation of ARF-1.2 and ARF-3 to affect UNC-97 level, myosin organization, and mobility

(A) Bar graph indicating that muscle-specific RNAi against *arf-1.2* or *arf-3* results in mobility defects.

(B–E) GFP images and bar graph showing that muscle-specific RNAi against *arf-1.2* or *arf-3* results in myosin disorganization.

(F and G) Western blots and bar graph showing that *arf-1.2(muscle-RNAi)* or *arf-3(muscle-RNAi)* treatments caused reduction in the level of UNC-97::GFP from the integrated transgene.

(H–K) Western blots and bar graphs indicating that myristoylation level of ARF-1.2 and ARF-3 in body-wall muscle of *acs-4(lf);acs-17(lf)* mutants was decreased. 1-day adults were analyzed.

(L–N) GFP images and bar graph showing that localization of body-wall-muscle-expressed ARF-1.2::GFP is changed in *acs-4(lf);acs-17(lf)* animals. Unlike the punctate distribution (red arrows) in some muscle cells of control animals, the ARF-1.2::GFP showed diffused distribution (white arrow) and clustering aggregates (red arrowhead) in some muscle cells of *acs-4(lf);acs-17(lf)* animals.

(O–Q) GFP images and bar graph showing that localization of body-wall-muscle-expressed ARF-3::GFP is changed in *acs-4(lf);acs-17(lf)* animals. Unlike the punctate (red arrows) and diffuse distribution of GFP in *acs-4(lf/+);acs-17(lf)* control animals, ARF-3::GFP puncta were not observed (white arrow) in *acs-4(lf);acs-17(lf)* animals.

(R and S) Western blots and bar graph showing myristoylation level of ARF-1.2::GFP from a signal-copy *myo-3p::arf-1.2::GFP* transgene is drastically reduced in wild-type animals treated with *fasn-1(RNAi)* to reduce overall FA level.

(T–V) GFP images and bar graph showing that the punctate distribution of ARF-1.2::GFP became mostly diffused in *fasn-1(RNAi)* animals (also see Figure S3B for localization on sarcomere).

(B–D, L–P, T, and U) Scale bars, 20 μm.

(A, E, G, I, K, N, Q, S, and V) Error bars, standard deviation. *$p < 0.05$.

(G, I, K, and S) Three biological replicates (n = 3) were performed and used for quantifications of the signals and are shown as means ± standard deviation. *$p < 0.05$.

consistent with the result from a previous RNAi screen that implicated a role for *arf-1.2* in sarcomere integrity (Etheridge et al., 2015). We then performed muscle-specific RNAi of *arf-1.2* and *arf-3* and observed mobility defects and disorganized myosin (Figures 3A–3E). Moreover, this treatment also resulted in a reduction of the UNC-97::GFP level (Figures 3F and 3G). Because myristoylation is required for functions of many membrane-bound proteins, including ARF guanosine triphosphatases (GTPases) (Liu et al., 2009; Resh, 2016), these data suggest a potential role of myristoylation of ARF-1.2 and ARF-3 in mediating the impact of FA metabolism on myosin organization and mobility.

We then evaluated protein myristoylation levels in strains carrying ARF-1.2::GFP and ARF-3::GFP transgenes and found that the myristoylation level of both transgenic proteins were reduced in the *acs-4(lf);acs-17(lf)* double mutants (Figures 3H–3K). In addition, these transgenes were expressed in the body-wall muscle and showed changes in GFP localization in *acs-4(lf);acs-17(lf)* double mutants (Figures 3L–3Q). Specifically, although ARF-1.2::GFP displayed punctate formation in the control animals, it was diffusely distributed and often formed aggregates in *acs-4(lf);acs-17(lf)* mutants (Figures 3L–3N). Similarly, for ARF-3::GFP, although puncta were observed in the control animals, a diffused distribution without puncta was observed in the *acs-4(lf);acs-17(lf)* double mutants (Figures 3O–3Q). In addition, we examined the impact of FA deprivation on ARF-1.2 myristoylation and localization by using a single-copy *myo-3p::arf-1.2::GFP* transgene (Figures 3R–3V). We observed that the ARF-1.2 myristoylation level in muscle was drastically reduced in *fasn-1(RNAi)*-treated worms (Figures 3R and 3S). In addition, the punctate distribution of the GFP signal in the cytoplasm and its presence in a striation pattern in sarcomeres was mostly lost in *fasn-1(RNAi)* animals (Figures 3T–3V and S3B). Taken together, our data suggest that FAs level may affect muscle integrity and animal mobility in part through regulating myristoylation of ARF-1.2 and ARF-3 that dictates their cellular localization.

FA deprivation and myristoylation deficiency induce ER stress

Because the imbalance of proteostasis in the ER is critically involved in degenerative diseases (Frakes and Dillin, 2017; Hetz and Saxena, 2017), we tested whether ER stress was induced by FA and myristoylation deficiency. ER stress triggers activation of three UPR^{ER} pathways to promote a number of downstream activities to recover ER protein homeostasis (Figure 4A; Wang and Kaufman, 2016). The Bip protein HSP-4 is transcriptionally induced by the IRE-1 pathway and commonly used as an ER stress marker (Calfon et al., 2002). We observed a drastic increase in *hsp-4p::GFP* expression in the body-wall muscle of the *acs-4(lf);acs-17(lf)* double mutants at L4 and adult stages, when the double mutants displayed mobility defects (Figures 4B–4E and S4A–S4H). Induction of *hsp-4::GFP* in body-wall muscle was also seen in animals treated with RNAi against *fasn-1*, *pod-2*, and *nmt-1* (Figures 4F–4M), correlating ER stress increase with the muscle and mobility defects under the same FA-deprivation and myristoylation-deficient conditions. We also observed an increase in *hsp-4p::GFP* expression in the seam cells of the *acs-4(lf);acs-17(lf)* double mutants (Figures S4G and S4H).

To identify specific myristoylated proteins that affect ER homeostasis, we also evaluated the effect of RNAi against genes for the 40 myristoylated proteins we identified (Table S1). ARF-1.2 and ARF-3 were the only two proteins that, when knocked down by RNAi, displayed both phenotypes (Figures 4F, 4I, 4J, and 4M; Table S2), supporting that these two GTPases play important roles in mediating the impact of FA deprivation on ER homeostasis.

To further demonstrate ER stress was induced by myristoylation deficiency, we also examined the activity of PEK-1/PERK that executes its UPR^{ER} function by phosphorylation of the translational initiation factor eIF2α (EIF-2a in *C. elegans*; Figure 4A). We constructed a muscle-specific transgene expressing a tagged EIF-2a (*myo-3p::eif-2a::FLAG::HA*) and observed a significant increase in phosphorylation of EIF-2a (p-EIF-2a) in the *acs-4(lf);acs-17(lf)* double mutants (Figures 4N–4P), and this increase was dependent on *pek-1*/PERK (Figure S4I), supporting that PERK is activated under myristoylation deficiency. Genetically, combining a *pek-1(lf)* mutation or *atf-6(RNAi)* with *acs-4(lf);acs-17(lf)* caused larval lethality (Figure S4J), which is consistent with ER stress being induced under the myristoylation-deficient condition and a pivotal role of UPR^{ER} in suppressing ER-stress-induced developmental defects (Shen et al., 2001).

ER stress mediates the impact of FA and myristoylation deficiency on sarcomere integrity and animal mobility

We then carried out several sets of experiments to determine whether ER stress actually mediates the impact of myristoylation deficiency on mobility, myosin organization, and *unc-97* expression. We first asked whether inducing ER stress by repressing both HSP-3 and HSP-4, two BiP proteins critical for maintaining proteostasis in the ER (Kapulkin et al., 2005; Shen et al., 2001; Walter and Ron, 2011), would cause similar muscle defects as those seen in myristoylation-deficient animals (Figure 1F). Indeed, the combination of *hsp-4(RNAi)* and a *hsp-3(lf)* mutation caused disorganized myosin, mobility defects, and reduced UNC-97::GFP level (Figures 5A–5F and S5A). In addition, enhancing ER stress in the *acs-4(lf);acs-17(lf)* double mutants by adding the *hsp-4(lf)* mutation caused paralysis at earlier stages (Figure S5B). The observation that *unc-97(RNAi)*, which causes muscle defects, did not cause ER stress (Figures 4L and 4M) is also consistent with the idea that reduction in *unc-97* expression and defective sarcomeres are downstream events of ER stress.

Second, we reasoned that, if ER stress is causal to the muscle defects in myristoylation-deficient animals, then reducing ER stress in these animals may suppress the defects to some extent. XBP-1 is a transcription factor that promotes ER homeostasis by activating genes involved in protein folding and unfolded protein degradation (Kapulkin et al., 2005; Shen et al., 2001; Walter and Ron, 2011; Figure 4A). Overexpression of a constitutively activated *xbp-1s* gene (spliced *xbp-1*) has been shown to ameliorate ER stress (Shen et al., 2001; Taylor and Dillin, 2013). We showed that driving the expression of *xbp-1s* by a ubiquitous promoter (*sur-5*) or a muscle-specific promoter (*unc-54*), but not a pan-neuronal promoter (*rab-3*), significantly suppressed the defects in myosin organization, mobility, and the UNC-97 level in *acs-4(lf);acs-17(lf)* animals (Figures 5G and S5C–S5G). In addition, we found *hsp-3(RNAi)* alone, which was reported to reduce ER stress by activating the negative feedback regulation of ER stress pathway (Hsu et al., 2003; Kapulkin et al., 2005), also significantly suppressed phenotypes in the *acs-4(lf);acs-17(lf)* double mutants, as the myosin disorganization and paralysis phenotypes were delayed for 2 days and UNC-97::GFP level increased (Figures 5H–5Q). These rescue effects indicated a critical role of ER stress in the onset of sarcomere disorganization and paralysis in myristoylation-defective animals.

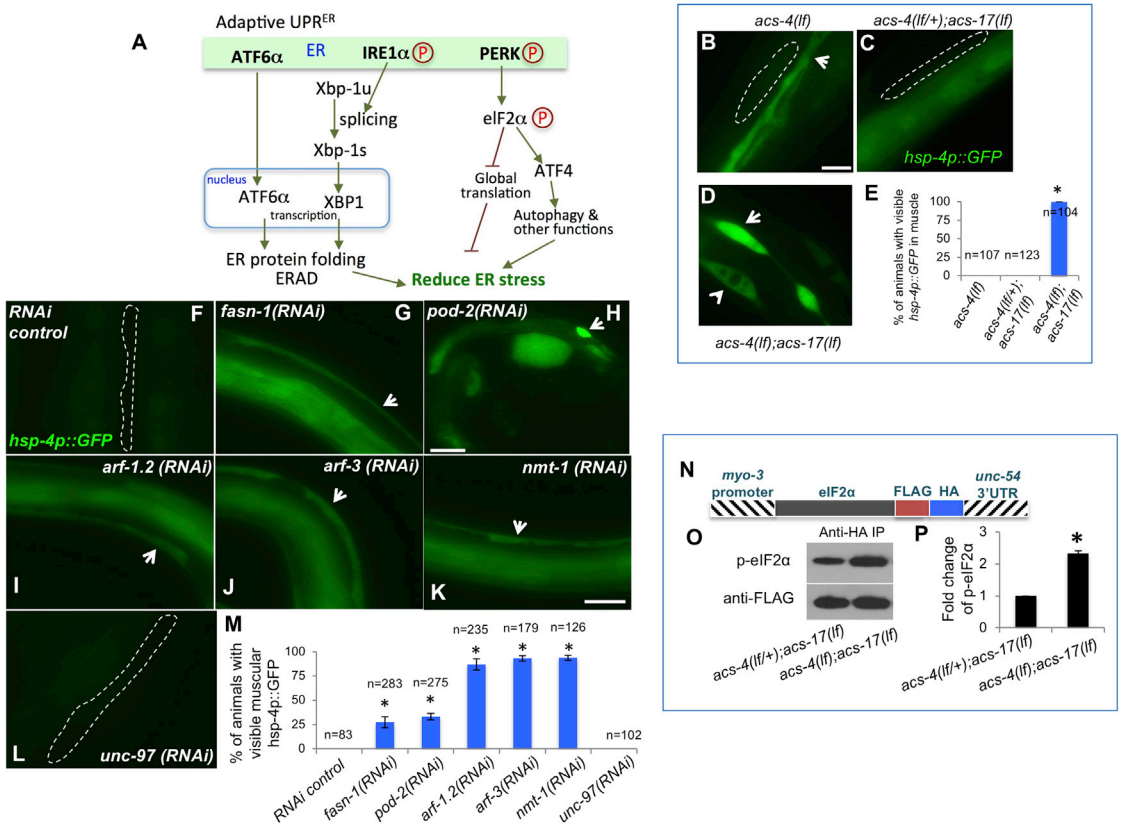

Figure 4. ER stress is critically involved in the impact of myristoylation deficiency on sarcomere integrity and animal mobility

(A) A simplified diagram showing the UPR^{ER} pathways (Wang and Kaufman, 2016). ERAD, ER-associated degradation.

(B–E) GFP images and bar graph showing that ER stress, marked by a *hsp-4p::GFP* reporter, is induced in the body-wall-muscle cells in the 1-day *acs-4(lf);acs-17(lf)* adults. ER stress was induced in seam cells in *acs-4(lf)* single mutant and *acs-4(lf);acs-17(lf)* double mutant (arrows in B and D). However, muscular ER stress was induced only in *acs-4(lf);acs-17(lf)* animals (arrowhead in D), but not in the animals with the other two genotypes (outlined). Scale bar, 20 μm.

(F–M) GFP images and bar graph showing that RNAi against *fasn-1*, *pod-2*, *arf-1.2*, *arf-3*, and *nmt-1*, but not *unc-97*, induces *hsp-4p::GFP* expression in the body-wall-muscle cells. ER stress was also observed in some other tissues, including intestine in (F)–(K). Arrows and dashed lines indicate body-wall-muscle cells. Animals were grown for 72 h post-hatch before scoring. Animals with visible GFP signal in body-wall-muscle cells were scored as positive. Scale bar, 20 μm. Error bars (E and M), standard deviation. *p < 0.05.

(N) Schematic drawing of an *elf-2a* transgene containing the *myo-3* promoter (body wall muscle specific), the 3′ UTR of unc-54/myosin, and tags of FLAG and hemagglutinin (HA).

(O and P) Western blots and bar graph showing that phosphorylated eIF-2a (p-eIF-2a), expressed from the transgene diagramed in (N), was increased in the body-wall muscle in 1-day *acs-4(lf);acs-17(lf)* adults. After anti-HA immunoprecipitation (IP), western blot was performed using either an anti-p-eIF2alpha antibody or an anti-FLAG antibody (input control).

(P) Three biological replicates (n = 3) were performed and used for quantifications of the signals and are shown as means ± standard deviation. *p < 0.05.

Third, similar to our observation in *acs-4(lf); acs-17(lf)* double mutants (Figure 5G), we found that alleviation of ER stress by expressing *xbp-1s* also significantly suppressed the mobility defects and raised the UNC-97::GFP level in *arf-1.2(muscle-RNAi)*- and *arf-3(muscle-RNAi)*-treated animals (Figures 5R, S5H, and S5I). Because RNAi of these two genes induced ER stress in body-wall muscle cells (Figure 4M), these data provide further support of the idea that myristoylation of these two small GTPases critically affects ER homeostasis that in turn regulates sarcomere integrity. Altogether, the above data indicate ER stress mediates the impacts of FA and myristoylation deficiency on muscle maintenance. Additional analyses suggest that mitochondrial stress or cytosolic proteotoxicity (D'Amico et al., 2017; Kim et al., 2016; Labbadia and Morimoto, 2015, Link et al., 1999) are not likely to play a major role in generating the paralysis phenotype in the *acs-4(lf);acs-17(lf)* double mutants (Figures S5J–S5T).

Phosphorylation of eIF-2a critically contributes to the impact of ER stress on sarcomere integrity

Upon acute ER stress, the three UPR^{ER} pathways act to protect the cells by increasing folding capacity and decreasing protein load in the ER (Walter and Ron, 2011; Wang and Kaufman, 2016; Figure 4A). However, under excessive or prolonged ER stress, UPR^{ER} can cause apoptosis and pathologic damage, and the PERK pathway plays critical roles in maladaptive UPR^{ER} (Martínez et al., 2017; Wang and Kaufman, 2016). We thus tested whether PERK activation, which was indicated by a prominent

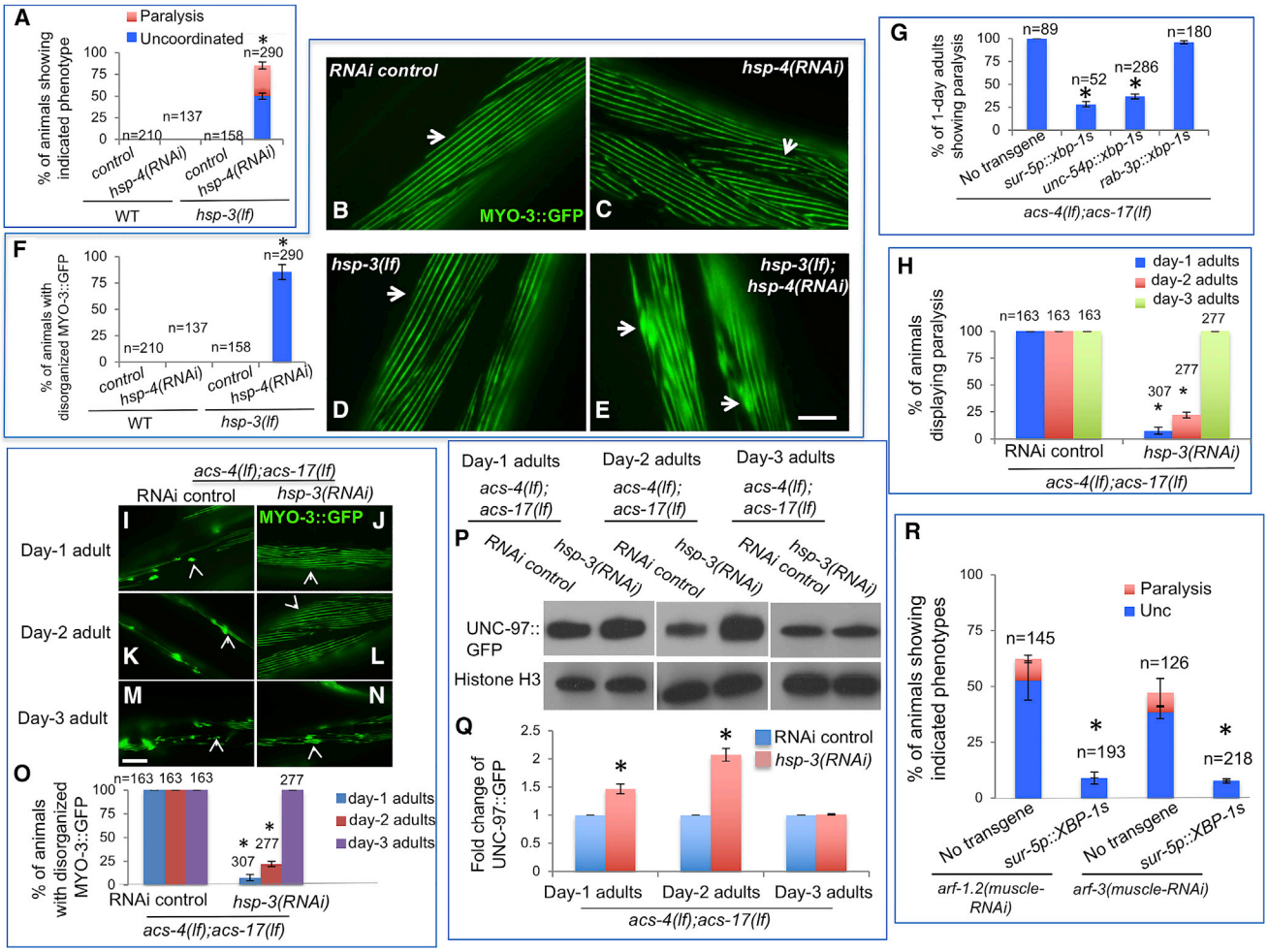

Figure 5. Alleviation of ER stress suppresses paralysis in myristoylation-deficient mutants

(A) Bar graph showing that combining *hsp-3(lf)* and *hsp-4(RNAi)* results in mobility defect.

(B–F) GFP images and bar graph indicating that *hsp-3* and *hsp-4* act redundantly to support normal myosin organization. Animals indicated in (A) were analyzed. Arrows in (E) indicate disorganized myosin.

(G) Bar graph showing that alleviation of ER stress by expressing the spliced *xbp-1* (*xbp-1s*) behind a ubiquitous (*sur-5*) or muscular (*unc-54*) promoter, but not a neuronal promoter (*rab-3*), suppressed the paralysis phenotype in the *acs-4(lf);acs-17(lf)* double mutants.

(H) Bar graph showing that *hsp-3(RNAi)* delays paralysis in the *acs-4(lf);acs-17(lf)* mutants.

(I–O) GFP images and bar graph indicating that normal myosin organization was recovered in the *acs-4(lf);acs-17(lf)* animals treated with *hsp-3(RNAi)*. All *hsp-3(RNAi)*-treated animals with delayed paralysis shown in (H) displayed recovered myosin filaments.

(P and Q) Western blots and bar graph indicating that the relative level of UNC-97 in the *acs-4(lf);acs-17(lf); hsp-3(RNAi)* animals with delayed paralysis was significantly increased. The relative level was calculated by normalizing to the RNAi control.

(Q) Three biological replicates (n = 3) were performed and used for quantifications of the signals and are shown as means ± SD. *p < 0.05.

(R) Bar graph indicating that alleviation of ER stress by overexpressing *xbp-1s* from a transgene containing Ex(*sur-5p::xbp-1s::let-858 3′UTR*) suppresses the mobility defects caused by *arf-1.2(muscle-RNAi)* or *arf-3(muscle-RNAi)*. Animals grown 72 h post-hatch (day 1 adults) after two generations of RNAi treatment were scored.

(B–E and I–N) Scale bars, 20 μm.

(A, F–H, O, and R) Error bars, standard deviation. *p < 0.05.

increase in *eIF-2a* phosphorylation (Figures 4N–4P), plays a critical role in mediating the effect of ER stress on muscle maintenance in myristoylation-deficient animals. To demonstrate that increase in *eIF-2a* phosphorylation can be causal to the sarcomere defects, we constructed a transgene expressing a phospho-mimetic version of eIF-2a, EIF-2a(S49D) (Nukazuka et al., 2008), specifically in body-wall muscle cells. Wild-type animals expressing EIF-2a(S49D) in muscle displayed prominent mobility defects, myosin disorganization, and UNC-97::GFP reduction (Figures 6A–6F). To detect the contribution of high PERK/eIF-2a activity to the muscle defects in myristoylation-deficient animals, we generated a muscle-specific transgene that expresses a phospho-dead version of EIF-2a, EIF-2a(S49A) (Nukazuka et al., 2008). We observed that *myo-3p::eIF-2a(S49A)*

significantly enhanced the effect of *xbp-1s* overexpression in suppressing the paralysis, myosin disorganization, and UNC-97 reduction phenotypes in *acs-4(lf);acs-17(lf)* mutants (Figures 6G–6L and S6A–S6F). In addition, treatment with a proteasome inhibitor, MG132, did not suppress the paralysis phenotype in the *acs-4(lf);acs-17(lf)* double mutants (Figure S6G), suggesting that proteasome-involved protein degradation may not play a major role in UNC-97 decrease and sarcomere disorganization. Therefore, translation inhibition by increased p-eIF-2a is likely causal to the paralysis phenotype in the *acs-4(lf);acs-17(lf)* double mutants.

We further tested the epistasis relationship between overexpression of *xbp-1s*, which reduces ER stress (Shen et al., 2001; Taylor and Dillin, 2013) and suppresses the paralysis phenotype in myristoylation-deficient animals (Figure 5G), and muscle-specific overexpression of the eIF-2a(S49D) phosphomimetic transgene, which causes the paralysis and muscle defects in wild type (Figures 6A–6D). We found that the rescue effects of expressing *xbp-1s* with muscle-specific transgenes (paralysis and UNC-97::GFP level in myristoylation-deficient animals) were eliminated by the EIF-2a(S49D) phospho-mimetic transgene (Figures 6J and 6K), indicating that the effect of *eIF2a* activation is epistatic to the *xbp-1s*-mediated functions at ER. These results support that eIF2a activation acts downstream of ER stress to cause sarcomere disorganization, further demonstrating a critical role of the PERK pathway in mediating role of ER homeostasis in muscle maintenance.

DISCUSSION

In this study, we discovered a mechanism by which FA metabolism profoundly impacts sarcomere integrity and animal mobility through regulating protein myristoylation and ER homeostasis (Figure 6L). Given the critical impact of nutrient levels on the onset of sarcopenia, the conserved sarcomere structure in *C. elegans* and mammals, and the critical role of ER homeostasis in aging and degenerative diseases (Herndon et al., 2002; Hetz and Saxena, 2017; Robinson et al., 2012; Wang and Kaufman, 2016), our finding may provide valuable insights into the pathogenesis of sarcopenia and muscle-degenerative diseases.

Muscle mass loss has been shown to be a major characteristic of aging-related muscle-function decline. Aging-induced alteration of various cellular processes, such as declined function of muscle stem cells and changes in Akt-mTOR signaling, ubiquitin-proteasome, and autophagy-lysosome system, critically contribute to muscle mass loss during sarcopenia (Masiero et al., 2009; Neel et al., 2013; Walston, 2012). Our data provide mechanistic insights into the impact of a poor nutritional condition (low FA level) on the pathogenesis of muscle degeneration. The breakdown of sarcomeres has been suggested to be a protective mechanism to ensure essential cellular functions by providing nutrients in response to prolonged starvation (Cahill, 1970), and the UPR^{ER} is known to play an important role in sensing the nutrition level and metabolic changes (Kaufman et al., 2002). Therefore, the critical involvement of ER homeostasis in modulating sarcomere integrity may serve as a mechanism for maintaining animal viability in response to nutrient deprivation and metabolic changes.

Our observation that mobility defects in the myristoylation-deficient animals started at a late developmental stage is consistent with previous reports that ER stress is increased with aging due to a declining capacity to cope with proteostatic stress (Ben-Zvi et al., 2009; Naidoo, 2009). Such a critical role of ER homeostasis in mobility is further supported by our data that alleviation of ER stress delayed paralysis in a subset of animals (Figures 5G and 5O) and increased ER stress caused earlier paralysis at larval stages (Figures S5B and S5C). However, the suppression of paralysis by alleviation of ER stress in the myristoylation-deficient animals only lasted for 1 to 2 days, implying that either some other pathways are involved in the pathogenesis of paralysis or exacerbated protein-folding problems that come with aging and continuous deficiency of myristoylation might overwhelm the function of *xbp-1s* overexpression in our system. Interestingly, ER homeostasis regulates sarcomere integrity autonomously in body-wall muscle (Figure 5G), which is different from its function in longevity through acting non-autonomously in neurons (Taylor and Dillin, 2013). Additionally, it was shown that altering FA saturation level and membrane fluidity by inactivating *mdt-15*, a transcription mediator that regulates the expression of FA desaturation genes, caused activation of UPR^{ER} without disturbing proteostasis (Hou et al., 2014). However, our data indicate that abnormal fat metabolism can also result in ER stress through affecting protein myristoylation (Figures 4B–4E and 4M), which is consistent with the observation that myristoylation affects ER homeostasis in human cells (Thinon et al., 2016), implying the complexity of fat metabolism function.

Myristoylation is required for all mammalian ARF proteins to perform biological functions (Liu et al., 2009), and thus, deficiency of myristoylation in ARF-1.2 and ARF-3 in *C. elegans* may compromise their functions in regulating membrane trafficking (Donaldson and Jackson, 2011), which could subsequently result in the failure of ER-processed proteins to concentrate at the ER exit sites and cause the imbalance of proteostasis in the ER (Lippincott-Schwartz et al., 2000). In addition, the imbalance in ER proteostasis and the reduced membrane trafficking could affect the normal localization of integrins to the muscle cell membrane, which may in turn contribute to the disruption of sarcomere integrity. Because alleviation of ER stress can partially suppress the mobility defects in myristoylation-deficient mutants (Figure 5G) and ARF-RNAi-treated animals (Figure 5R), lack of myristoylation in ARFs may cause mobility defects at least partially through affecting ER homeostasis. Although certain chaperones have been known to help correct folding of sarcomere proteins (Barral et al., 1998; Moerman and Williams, 2006; Papsdorf et al., 2014), none of these genetic mutants showed the same phenotype as observed in myristoylation-deficient animals, suggesting that these chaperones are not critically involved in the ER homeostasis-mediated regulation of sarcomere integrity.

As a component of the integrin-based attachment complex, the role of UNC-97/PINCH in modulating sarcomere integrity in response to FA metabolism change is intriguing, as it was reported to respond to spaceflight (Etheridge et al., 2012). UNC-97 was identified as a negative regulator of muscle protein degradation (Shephard et al., 2011), which is consistent with the idea that downregulation of *unc-97* promotes sarcomere

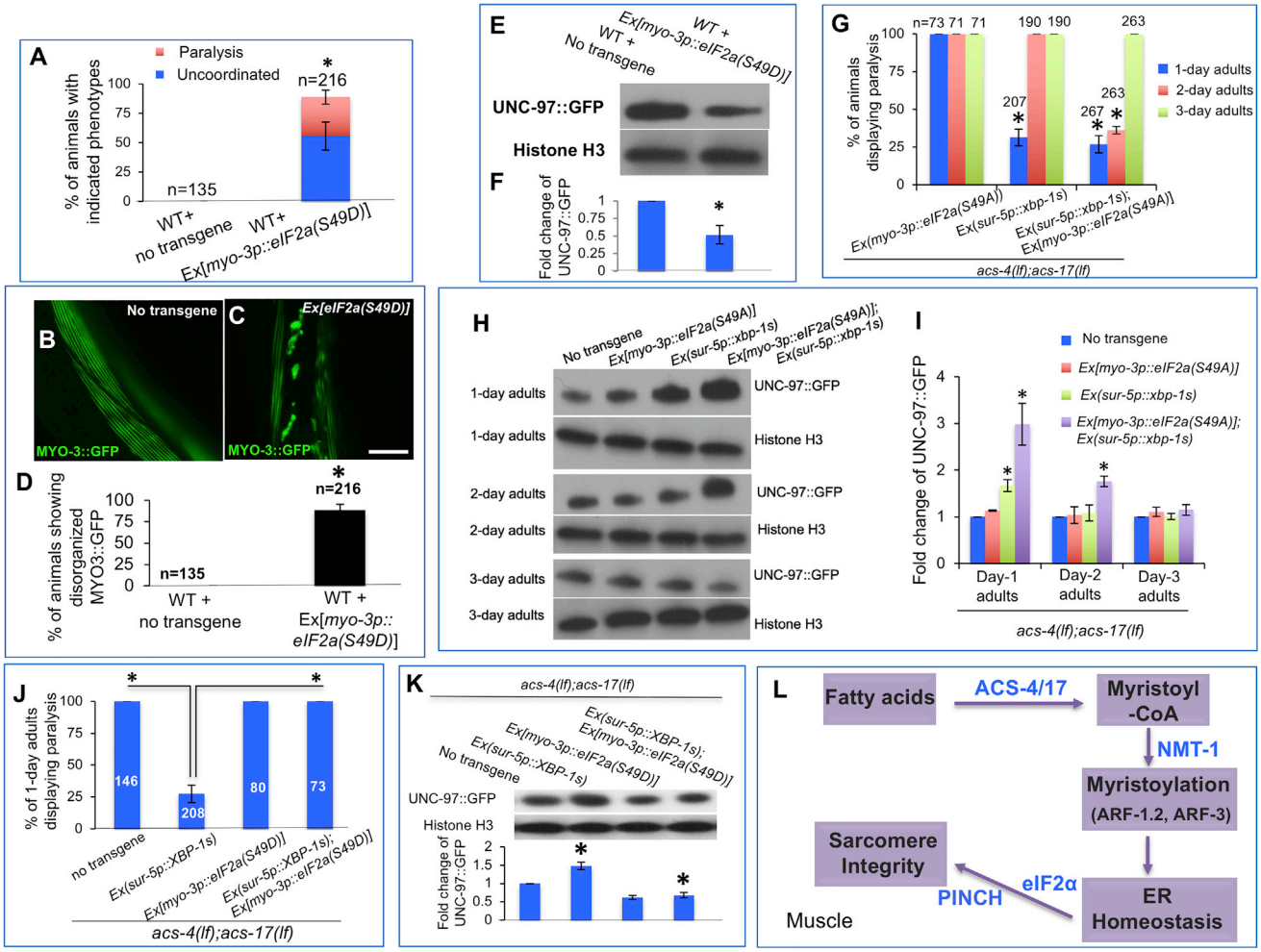

Figure 6. Translation initiation factor eIF-2a is critically involved in the impact of myristoylation on UNC-97 expression, sarcomere integrity, and animal mobility

(A) Bar graph showing that the body-wall-muscle-expressed phospho-mimetic version of eIF-2a, eIF-2a(S49D), causes mobility defects in wild-type animals.

(B–D) GFP images and bar graph showing that body-wall-muscle-expressed eIF-2a(S49D) disrupts myosin organization. This defect was observed in all animals displaying mobility defects in (A). Scale bar, 20 μm.

(E and F) Western blots and bar graph showing that muscle-specific expression of *eIF-2a(S49D)* causes reduction in UNC-97 level in 1-day adults, indicating a dominant-negative effect of this mutant gene. 1-day adults were analyzed, and the paralyzed and/or uncoordinated animals expressing eIF-2a(S49D) were collected for western blotting.

(G) Bar graph showing that muscle-specific expression of a phospho-dead version of *eIF-2a*, *eIF-2a(S49A)*, enhances the effect of overexpression of *xbp-1s* in delaying paralysis in *acs-4(lf);acs-17(lf)* mutants (delay the paralysis phenotype for 1 additional day).

(H and I) Western blots and bar graph showing that muscle-specific expression of *eIF-2a(S49A)* significantly enhanced the effect of the overexpressed *xbp-1s* in raising the UNC-97 level in *acs-4(lf);acs-17(lf)* animals.

(J) Bar graph showing that the delayed paralysis in *acs-4(lf);acs-17(lf)* mutants by overexpressing *xbp-1s* was eliminated by muscle-specific expression of the eIF-2a(S49D) mutant protein.

(K) Western blots and bar graph showing that recovery of UNC-97 level in *acs-4(lf);acs-17(lf)* day-1 adults by overexpressing *xbp-1s* was eliminated by muscle-specific expression of eIF-2a(S49D).

(L) The proposed model for the mechanism underlying the functions of FAs in maintaining sarcomere integrity. Protein myristoylation mediates the impact of fatty acids on sarcomere maintenance through affecting ER homeostasis that regulates UNC-97/PINCH level via phosphorylating eIF-2a.

(E, F, H, I, and K) Three biological replicates (n = 3) for western blots were performed and used for quantifications of the signals and are shown as means ± standard deviation. *$p < 0.05$.

(A, D, G, and J) Error bars, standard deviation. *$p < 0.05$.

breakdown in response to food and FA deprivation. In addition, UNC-97 also functions as a signaling platform for interfacing with various signaling pathways by interacting with integrin-like kinase and parvin (Legate et al., 2006). It is reported that decreasing integrin signaling by reducing the function of ILK, actopaxin, or β-integrin delayed functional senescence in both

C. elegans and *Drosophila* (Goddeeris et al., 2003; Kumsta et al., 2014). Therefore, downregulation of *unc-97* by UPR^{ER} may represent a protective mechanism to respond to nutrient deprivation through delaying functional senescence and promoting muscle breakdown. However, the underlying biochemical mechanism by which *unc-97*/PINCH expression is downregulated by myristoylation deficiency and ER stress is not clear, and addressing this question may be a key toward fully understanding how FA availability impacts muscle sarcomere integrity.

Although we have shown strong evidence that myristoylation plays a critical role in maintaining sarcomere integration, we do not have data to show this response applies to FA level changes under specific physiological conditions, such as starvation and aging. These will be challenging but important questions to address in future studies.

STAR★METHODS

Detailed methods are provided in the online version of this paper and include the following:

- KEY RESOURCES TABLE
- RESOURCE AVAILABILITY
  - Lead contact
  - Materials availability
  - Data and code availability
- EXPERIMENTAL MODEL AND SUBJECT DETAILS
- METHOD DETAILS
  - Characterization of paralysis, the uncoordinated phenotype, sarcomere structure and ER stress
  - RNAi by feeding and injection
  - Construction of transgenes
  - Analysis of larval lethality
  - Western blotting
  - Immunostaining
  - Analysis of myristoylated proteins
  - Analysis of ARF-1.2 and ARF-3 myristoylation
- QUANTIFICATION AND STATISTICAL ANALYSIS

SUPPLEMENTAL INFORMATION

Supplemental information can be found online at https://doi.org/10.1016/j.celrep.2021.109539.

ACKNOWLEDGMENTS

We thank Guy Benian, Kathrin Gieseler, Andrew Dillin, Shin Takagi, and Richard Kahn for reagents; CGC (funded by NIH [P40OD010440]) for strains; Will Old and Brad Olwin for advice; Aileen Sewell for critical comments and editing; and Han lab members for helpful discussions. This work was supported by NIH R01 grant (1R01AR074503; M.H.) and the Howard Hughes Medical Institute (M.H., H.T., and M.C.).

AUTHOR CONTRIBUTIONS

H.T. and M.C. designed the research, performed the experiments, analyzed data, and wrote the manuscript; M.H. supervised the study and edited the paper.

DECLARATION OF INTERESTS

The authors declare no competing interests.

Received: October 7, 2020
Revised: June 4, 2021
Accepted: July 26, 2021
Published: August 17, 2021

SUPPORTING CITATIONS

The following references appear in the supplemental information: Baird et al. (2014); Benedetti et al. (2006); Morley and Morimoto (2004); Shen et al. (2005).

REFERENCES

Baird, N.A., Douglas, P.M., Simic, M.S., Grant, A.R., Moresco, J.J., Wolff, S.C., Yates, J.R., 3rd, Manning, G., and Dillin, A. (2014). HSF-1-mediated cytoskeletal integrity determines thermotolerance and life span. Science *346*, 360–363.

Barral, J.M., Bauer, C.C., Ortiz, I., and Epstein, H.F. (1998). Unc-45 mutations in Caenorhabditis elegans implicate a CRO1/She4p-like domain in myosin assembly. J. Cell Biol. *143*, 1215–1225.

Ben-Zvi, A., Miller, E.A., and Morimoto, R.I. (2009). Collapse of proteostasis represents an early molecular event in Caenorhabditis elegans aging. Proc. Natl. Acad. Sci. USA *106*, 14914–14919.

Benedetti, C., Haynes, C.M., Yang, Y., Harding, H.P., and Ron, D. (2006). Ubiquitin-like protein 5 positively regulates chaperone gene expression in the mitochondrial unfolded protein response. Genetics *174*, 229–239.

Bohnert, K.R., McMillan, J.D., and Kumar, A. (2018). Emerging roles of ER stress and unfolded protein response pathways in skeletal muscle health and disease. J. Cell. Physiol. *233*, 67–78.

Cahill, G.F., Jr. (1970). Starvation in man. N. Engl. J. Med. *282*, 668–675.

Calfon, M., Zeng, H., Urano, F., Till, J.H., Hubbard, S.R., Harding, H.P., Clark, S.G., and Ron, D. (2002). IRE1 couples endoplasmic reticulum load to secretory capacity by processing the XBP-1 mRNA. Nature *415*, 92–96.

Campagnola, P.J., Millard, A.C., Terasaki, M., Hoppe, P.E., Malone, C.J., and Mohler, W.A. (2002). Three-dimensional high-resolution second-harmonic generation imaging of endogenous structural proteins in biological tissues. Biophys. J. *82*, 493–508.

D'Amico, D., Sorrentino, V., and Auwerx, J. (2017). Cytosolic proteostasis networks of the mitochondrial stress response. Trends Biochem. Sci. *42*, 712–725.

Dickinson, D.J., and Goldstein, B. (2016). CRISPR-based methods for Caenorhabditis elegans genome engineering. Genetics *202*, 885–901.

Dickinson, D.J., Ward, J.D., Reiner, D.J., and Goldstein, B. (2013). Engineering the Caenorhabditis elegans genome using Cas9-triggered homologous recombination. Nat. Methods *10*, 1028–1034.

Donaldson, J.G., and Jackson, C.L. (2011). ARF family G proteins and their regulators: roles in membrane transport, development and disease. Nat. Rev. Mol. Cell Biol. *12*, 362–375.

Espelt, M.V., Estevez, A.Y., Yin, X., and Strange, K. (2005). Oscillatory Ca2+ signaling in the isolated Caenorhabditis elegans intestine: role of the inositol-1,4,5-trisphosphate receptor and phospholipases C beta and gamma. J. Gen. Physiol. *126*, 379–392.

Etheridge, T., Oczypok, E.A., Lehmann, S., Fields, B.D., Shephard, F., Jacobson, L.A., and Szewczyk, N.J. (2012). Calpains mediate integrin attachment complex maintenance of adult muscle in Caenorhabditis elegans. PLoS Genet. *8*, e1002471.

Etheridge, T., Rahman, M., Gaffney, C.J., Shaw, D., Shephard, F., Magudia, J., Solomon, D.E., Milne, T., Blawzdziewicz, J., Constantin-Teodosiu, D., et al. (2015). The integrin-adhesome is required to maintain muscle structure, mitochondrial ATP production, and movement forces in Caenorhabditis elegans. FASEB J. *29*, 1235–1246.

Evans, T.C. (2006). Transformation and microinjection. WormBook, 1–15.

Frakes, A.E., and Dillin, A. (2017). The UPR^{ER}: sensor and coordinator of organismal homeostasis. Mol. Cell *66*, 761–771.

Galvin, B.D., Li, Z., Villemaine, E., Poole, C.B., Chapman, M.S., Pollastri, M.P., Wyatt, P.G., and Carlow, C.K. (2014). A target repurposing approach identifies N-myristoyltransferase as a new candidate drug target in filarial nematodes. PLoS Negl. Trop. Dis. *8*, e3145.

Gieseler, K., Qadota, H., and Benian, G.M. (2017). Development, structure, and maintenance of C. elegans body wall muscle. WormBook, 1–59.

Goddeeris, M.M., Cook-Wiens, E., Horton, W.J., Wolf, H., Stoltzfus, J.R., Borrusch, M., and Grotewiel, M.S. (2003). Delayed behavioural aging and altered mortality in Drosophila beta integrin mutants. Aging Cell *2*, 257–264.

Herndon, L.A., Schmeissner, P.J., Dudaronek, J.M., Brown, P.A., Listner, K.M., Sakano, Y., Paupard, M.C., Hall, D.H., and Driscoll, M. (2002). Stochastic and genetic factors influence tissue-specific decline in ageing C. elegans. Nature *419*, 808–814.

Hetz, C., and Saxena, S. (2017). ER stress and the unfolded protein response in neurodegeneration. Nat. Rev. Neurol. *13*, 477–491.

Hobert, O., Moerman, D.G., Clark, K.A., Beckerle, M.C., and Ruvkun, G. (1999). A conserved LIM protein that affects muscular adherens junction integrity and mechanosensory function in Caenorhabditis elegans. J. Cell Biol. *144*, 45–57.

Hou, N.S., Gutschmidt, A., Choi, D.Y., Pather, K., Shi, X., Watts, J.L., Hoppe, T., and Taubert, S. (2014). Activation of the endoplasmic reticulum unfolded protein response by lipid disequilibrium without disturbed proteostasis in vivo. Proc. Natl. Acad. Sci. USA *111*, E2271–E2280.

Hsu, A.L., Murphy, C.T., and Kenyon, C. (2003). Regulation of aging and age-related disease by DAF-16 and heat-shock factor. Science *300*, 1142–1145.

Jose, A.M., Smith, J.J., and Hunter, C.P. (2009). Export of RNA silencing from C. elegans tissues does not require the RNA channel SID-1. Proc. Natl. Acad. Sci. USA *106*, 2283–2288.

Kapulkin, W.J., Hiester, B.G., and Link, C.D. (2005). Compensatory regulation among ER chaperones in C. elegans. FEBS Lett. *579*, 3063–3068.

Kaufman, R.J., Scheuner, D., Schröder, M., Shen, X., Lee, K., Liu, C.Y., and Arnold, S.M. (2002). The unfolded protein response in nutrient sensing and differentiation. Nat. Rev. Mol. Cell Biol. *3*, 411–421.

Kim, H.E., Grant, A.R., Simic, M.S., Kohnz, R.A., Nomura, D.K., Durieux, J., Riera, C.E., Sanchez, M., Kapernick, E., Wolff, S., et al. (2016). Lipid biosynthesis coordinates a mitochondrial-to-cytosolic stress response. Cell *166*, 1539–1552.e16.

Kumsta, C., Ching, T.T., Nishimura, M., Davis, A.E., Gelino, S., Catan, H.H., Yu, X., Chu, C.C., Ong, B., Panowski, S.H., et al. (2014). Integrin-linked kinase modulates longevity and thermotolerance in C. elegans through neuronal control of HSF-1. Aging Cell *13*, 419–430.

Labbadia, J., and Morimoto, R.I. (2015). The biology of proteostasis in aging and disease. Annu. Rev. Biochem. *84*, 435–464.

Labouesse, M., and Georges-Labouesse, E. (2003). Cell adhesion: parallels between vertebrate and invertebrate focal adhesions. Curr. Biol. *13*, R528–R530.

Laforêt, P., and Vianey-Saban, C. (2010). Disorders of muscle lipid metabolism: diagnostic and therapeutic challenges. Neuromuscul. Disord. *20*, 693–700.

Lee, K.Z., Kniazeva, M., Han, M., Pujol, N., and Ewbank, J.J. (2010). The fatty acid synthase fasn-1 acts upstream of WNK and Ste20/GCK-VI kinases to modulate antimicrobial peptide expression in C. elegans epidermis. Virulence *1*, 113–122.

Legate, K.R., Montañez, E., Kudlacek, O., and Fässler, R. (2006). ILK, PINCH and parvin: the tIPP of integrin signalling. Nat. Rev. Mol. Cell Biol. *7*, 20–31.

Lin, X., Qadota, H., Moerman, D.G., and Williams, B.D. (2003). C. elegans PAT-6/actopaxin plays a critical role in the assembly of integrin adhesion complexes in vivo. Curr. Biol. *13*, 922–932.

Link, C.D., Cypser, J.R., Johnson, C.J., and Johnson, T.E. (1999). Direct observation of stress response in Caenorhabditis elegans using a reporter transgene. Cell Stress Chaperones *4*, 235–242.

Lipina, C., and Hundal, H.S. (2017). Lipid modulation of skeletal muscle mass and function. J. Cachexia Sarcopenia Muscle *8*, 190–201.

Lippincott-Schwartz, J., Roberts, T.H., and Hirschberg, K. (2000). Secretory protein trafficking and organelle dynamics in living cells. Annu. Rev. Cell Dev. Biol. *16*, 557–589.

Liu, Y., Kahn, R.A., and Prestegard, J.H. (2009). Structure and membrane interaction of myristoylated ARF1. Structure *17*, 79–87.

Martínez, G., Duran-Aniotz, C., Cabral-Miranda, F., Vivar, J.P., and Hetz, C. (2017). Endoplasmic reticulum proteostasis impairment in aging. Aging Cell *16*, 615–623.

Masiero, E., Agatea, L., Mammucari, C., Blaauw, B., Loro, E., Komatsu, M., Metzger, D., Reggiani, C., Schiaffino, S., and Sandri, M. (2009). Autophagy is required to maintain muscle mass. Cell Metab. *10*, 507–515.

Meissner, B., Warner, A., Wong, K., Dube, N., Lorch, A., McKay, S.J., Khattra, J., Rogalski, T., Somasiri, A., Chaudhry, I., et al. (2009). An integrated strategy to study muscle development and myofilament structure in Caenorhabditis elegans. PLoS Genet. *5*, e1000537.

Melo, J.A., and Ruvkun, G. (2012). Inactivation of conserved C. elegans genes engages pathogen- and xenobiotic-associated defenses. Cell *149*, 452–466.

Mergoud Dit Lamarche, A., Molin, L., Pierson, L., Mariol, M.C., Bessereau, J.L., Gieseler, K., and Solari, F. (2018). UNC-120/SRF independently controls muscle aging and lifespan in Caenorhabditis elegans. Aging Cell *17*, 17.

Moerman, D.G., and Fire, A. (1997). Muscle: structure, function, and development. In C. elegans II, D.L. Riddle, T. Blumenthal, B.J. Meyer, and J.R. Priess, eds. (Cold Spring Harbor).

Moerman, D.G., and Williams, B.D. (2006). Sarcomere assembly in C. elegans muscle. WormBook, 1–16.

Morley, J.F., and Morimoto, R.I. (2004). Regulation of longevity in Caenorhabditis elegans by heat shock factor and molecular chaperones. Mol. Biol. Cell *15*, 657–664.

Naidoo, N. (2009). The endoplasmic reticulum stress response and aging. Rev. Neurosci. *20*, 23–37.

Neel, B.A., Lin, Y., and Pessin, J.E. (2013). Skeletal muscle autophagy: a new metabolic regulator. Trends Endocrinol. Metab. *24*, 635–643.

Norman, K.R., Cordes, S., Qadota, H., Rahmani, P., and Moerman, D.G. (2007). UNC-97/PINCH is involved in the assembly of integrin cell adhesion complexes in Caenorhabditis elegans body wall muscle. Dev. Biol. *309*, 45–55.

Nukazuka, A., Fujisawa, H., Inada, T., Oda, Y., and Takagi, S. (2008). Semaphorin controls epidermal morphogenesis by stimulating mRNA translation via eIF2alpha in Caenorhabditis elegans. Genes Dev. *22*, 1025–1036.

Papsdorf, K., Sacherl, J., and Richter, K. (2014). The balanced regulation of Hsc70 by DNJ-13 and UNC-23 is required for muscle functionality. J. Biol. Chem. *289*, 25250–25261.

Qadota, H., Mercer, K.B., Miller, R.K., Kaibuchi, K., and Benian, G.M. (2007). Two LIM domain proteins and UNC-96 link UNC-97/pinch to myosin thick filaments in Caenorhabditis elegans muscle. Mol. Biol. Cell *18*, 4317–4326.

Qadota, H., Moerman, D.G., and Benian, G.M. (2012). A molecular mechanism for the requirement of PAT-4 (integrin-linked kinase (ILK)) for the localization of UNC-112 (Kindlin) to integrin adhesion sites. J. Biol. Chem. *287*, 28537–28551.

Rappleye, C.A., Tagawa, A., Le Bot, N., Ahringer, J., and Aroian, R.V. (2003). Involvement of fatty acid pathways and cortical interaction of the pronuclear complex in Caenorhabditis elegans embryonic polarity. BMC Dev. Biol. *3*, 8.

Resh, M.D. (2016). Fatty acylation of proteins: the long and the short of it. Prog. Lipid Res. *63*, 120–131.

Reznick, D.N., and Braun, B. (1987). Fat cycling in the mosquitofish (Gambusia affinis): fat storage as a reproductive adaptation. Oecologia *73*, 401–413.

Robinson, S., Cooper, C., and Aihie Sayer, A. (2012). Nutrition and sarcopenia: a review of the evidence and implications for preventive strategies. J. Aging Res. *2012*, 510801.

Rogalski, T.M., Mullen, G.P., Gilbert, M.M., Williams, B.D., and Moerman, D.G. (2000). The UNC-112 gene in Caenorhabditis elegans encodes a novel component of cell-matrix adhesion structures required for integrin localization in the muscle cell membrane. J. Cell Biol. *150*, 253–264.

Rüegg, M.A., and Glass, D.J. (2011). Molecular mechanisms and treatment options for muscle wasting diseases. Annu. Rev. Pharmacol. Toxicol. *51*, 373–395.

Saini-Chohan, H.K., Mitchell, R.W., Vaz, F.M., Zelinski, T., and Hatch, G.M. (2012). Delineating the role of alterations in lipid metabolism to the pathogenesis of inherited skeletal and cardiac muscle disorders: thematic review series: genetics of human lipid diseases. J. Lipid Res. *53*, 4–27.

Shen, X., Ellis, R.E., Lee, K., Liu, C.Y., Yang, K., Solomon, A., Yoshida, H., Morimoto, R., Kurnit, D.M., Mori, K., and Kaufman, R.J. (2001). Complementary signaling pathways regulate the unfolded protein response and are required for C. elegans development. Cell *107*, 893–903.

Shen, X., Ellis, R.E., Sakaki, K., and Kaufman, R.J. (2005). Genetic interactions due to constitutive and inducible gene regulation mediated by the unfolded protein response in C. elegans. PLoS Genet. *1*, e37.

Shephard, F., Adenle, A.A., Jacobson, L.A., and Szewczyk, N.J. (2011). Identification and functional clustering of genes regulating muscle protein degradation from amongst the known C. elegans muscle mutants. PLoS ONE *6*, e24686.

Tabebordbar, M., Wang, E.T., and Wagers, A.J. (2013). Skeletal muscle degenerative diseases and strategies for therapeutic muscle repair. Annu. Rev. Pathol. *8*, 441–475.

Tang, H., and Han, M. (2017). Fatty acids regulate germline sex determination through ACS-4-dependent myristoylation. Cell *169*, 457–469.e13.

Taylor, R.C., and Dillin, A. (2013). XBP-1 is a cell-nonautonomous regulator of stress resistance and longevity. Cell *153*, 1435–1447.

Thinon, E., Morales-Sanfrutos, J., Mann, D.J., and Tate, E.W. (2016). N-myristoyltransferase inhibition induces ER-stress, cell cycle arrest, and apoptosis in cancer cells. ACS Chem. Biol. *11*, 2165–2176.

Walston, J.D. (2012). Sarcopenia in older adults. Curr. Opin. Rheumatol. *24*, 623–627.

Walter, P., and Ron, D. (2011). The unfolded protein response: from stress pathway to homeostatic regulation. Science *334*, 1081–1086.

Wang, M., and Kaufman, R.J. (2016). Protein misfolding in the endoplasmic reticulum as a conduit to human disease. Nature *529*, 326–335.

Warner, A., Xiong, G., Qadota, H., Rogalski, T., Vogl, A.W., Moerman, D.G., and Benian, G.M. (2013). CPNA-1, a copine domain protein, is located at integrin adhesion sites and is required for myofilament stability in Caenorhabditis elegans. Mol. Biol. Cell *24*, 601–616.

Waterston, R.H. (1988). The Nematode Caenorhabditis elegans (Cold Spring Harbor).

Wehrle-Haller, B., and Imhof, B. (2002). The inner lives of focal adhesions. Trends Cell Biol. *12*, 382–389.

Yochem, J., Gu, T., and Han, M. (1998). A new marker for mosaic analysis in Caenorhabditis elegans indicates a fusion between hyp6 and hyp7, two major components of the hypodermis. Genetics *149*, 1323–1334.

STAR★METHODS

KEY RESOURCES TABLE

REAGENT or RESOURCE	SOURCE	IDENTIFIER
Antibodies		
Mouse monoclonal anti-GFP antibody (JL-8)	Clontech	Cat #632381; RRID:AB_2313808
Anti-Histone H3 antibody	Abcam	Cat #Ab1791; RRID: AB_302613
Monoclonal ANTI-FLAG M2 antibody	Sigma-Aldrich	Cat# F3165, RRID:AB_259529
Anti-phospho-eIF2alpha^{S51}(Rabbit polyclonal)	Cell Signaling Technology	Cat #9721; RRID:AB_330951
Anti-PAT-4 antibody (Rabbit polyclonal)	Guy Benian lab (Emory University)	N/A
	Qadota et al., 2012	
Anti-PAT-6 antibody (Rat polyclonal)	Guy Benian lab (Emory University)	N/A
	Warner et al., 2013	
Bacterial and virus strains		
Escherichia coli OP50	Caenorhabditis Genetics Center (CGC)	N/A
Escherichia coli HT115(DE3)	CGC	N/A
RNAI feeding bacterial strain HT115(DE3)	Source BioScience	N/A
RNAI feeding bacterial strain HT115(DE3)	GE Dharmacon (ORF RNAi library)	N/A
Chemicals, peptides, and recombinant proteins		
Myristic acid alkyne	Cayman Chemical	Cat #13267
C-18 resin column	Pierce	Cat#89870
Dde Azide-agarose resin	Click Chemistry Tools	Cat #1153
Alexa Fluor 546 phalloidin	ThermoFisher	Cat#A22283
Critical commercial assays		
Click reaction kit	Click Chemistry Tools	Cat #1001
Azide agarose beads	Click Chemistry Tools	Cat#1038-2
MEGAscript T7 transcription kit	ThermoFisher	Cat #AM1334
Experimental models: organisms/strains		
C. elegans: N2 (Bristol), Wild type	Caenorhabditis Genetics Center (CGC)	N/A
C. elegans: acs-4(ok2872)	CGC	N/A
C. elegans: acs-17(ok1562)	CGC	N/A
C. elegans: stEx30 [myo-3p::GFP::myo-3 + rol-6(su1006)]	CGC	N/A
C. elegans: KAG420 (*kagIs4[gfp::myo-3, V:12226816]*)	Kathrin Gieseler (Université Claude Bernard – Lyon)	N/A
	Mergoud Dit Lamarche et al., 2018	
C. elegans: SJ4005 (*zcIs[hsp-4::GFP]*)	CGC	N/A
C. elegans: SJ4100 (*zcIs13(hsp-6p::GFP)*	CGC	N/A
C. elegans: TJ375 (*gpIs1(hsp-16.2p::GFP*)	CGC	N/A
C. elegans: OH122 (*mgIs25(unc-97::GFP)*)	CGC	N/A
C. elegans: RB1104 (*hsp-3(ok1083)*)	CGC	N/A
C. elegans: VC1099 (*hsp-4(gk514)*)	CGC	N/A
C. elegans: RB545 (*pek-1(ok275)*)	CGC	N/A
C. elegans: AGD710 (*uthIs235 [sur-5p::hsf-1::unc-54 3′UTR + myo-2p::tdTomato::unc-54 3′ UTR]*)	CGC	N/A
C. elegans: AGD927 (*uthIs270 [rab-3p::xbp-1 s (constitutively active) + myo-2p::tdTomato]*)	CGC	N/A

(*Continued on next page*)

Continued

REAGENT or RESOURCE	SOURCE	IDENTIFIER
C. elegans: SPC272 (*sid-1(qt9); Is(myo-3p::SID-1)*)	Gary Ruvkun Lab, Melo and Ruvkun, 2012	N/A
C. elegans: VP303 (*rde-1(ne219); kbIs7[nhx-2p::rde-1 + rol-6(su1006)]*)	CGC	N/A
C. elegans: NK358 (*unc-119(ed4); qyIs43[pat-3::GFP + ina-1(genomic) + unc-119(+)]*)	CGC	N/A
C. elegans: WB141 (*pat-6(st561); zpEx99[pat-6::GFP + rol-6(su1006)]*)	CGC	N/A
C. elegans: DM5115 (*unc-112(st581); raEx16[unc-112::GFP + rol-6(su1006)]*)	CGC	N/A
Oligonucleotides		
acs-4 promoter primer forward: 5′- AGTCAGTCGA CGATAATGCAGGATTGCCTCCCGTTATTAT −3′ (Sal I) −3′	This paper	N/A
acs-4 promoter primer reverse: 5′-CGGCGGCGGT CTAGACTGTAAATAACGAAAATTAGAAGAG −3′ (Xba I)	This paper	N/A
acs-4 cDNA primer forward: 5′- GCGTCTAGAATG AAACGGAAAGTTTCGGTATACG-3′ (Xba I)	This paper	N/A
acs-4 cDNA primer reverse: 5′- GCGTGCGGCC GCTTAATTCTTTTTGAGCTGCTT-3′ (Not I)	This paper	N/A
arf-1.2 genomic DNA primer forward: 5′-GCGCTT AATTAATGGGAAACGTGTTCGGCA-GCTT ATTT-3′	This paper	N/A
arf-1.2 genomic DNA primer reverse: 5′-GACTGT CGACAGATCTATTCTTGAGCTGGTTGCTGAG-3′	This paper	N/A
arf-3 genomic DNA primer forward: 5′- GCGCTTA ATTAATGGGTTTA-ACAATCTCCTCCCTCTTC-3′	This paper	N/A
arf-3 genomic DNA primer reverse: 5′- ATATGTC GACGGTCTTGGAAAGCTGGTTGGA-TA GC CAG-3′	This paper	N/A
hsp-4 genomic DNA primer forward: 5′- GCGCG CGCTTAATTAATGAAAGTTTTCTCGTT GATTTTGA-3′	This paper	N/A
hsp-4 genomic DNA primer reverse: 5′- AAGC AAGCTAGCTTACAGTTCATCATGATCCTCC GAT-3′	This paper	N/A
unc-97 primer forward: 5′- ATATATGGCGCGC CGTACGGAAGGCGCCAATAGCAC-3′(Asc I)	This paper	N/A
unc-97 primer reverse: 5′- ACACACGCTAGCT TATTTTGGTCCAGGACTCATCGA-3′ (Nhe I)	This paper	N/A
Recombinant DNA		
Plasmid: pPD95.77	pPD95.77 was a gift from Andrew Fire	Addgene Plasmid #1495
acs-4p::acs-4cDNA::GFP::let-858 3′UTR	This paper	N/A
myo-3p::acs-4cDNA::GFP::let-858 3′UTR	This paper	N/A
rgef-1p::acs-4cDNA::GFP::let-858 3′UTR	This paper	N/A
col-10p::acs-4cDNA::GFP::let-858 3′UTR	This paper	N/A
ges-1p::acs-4cDNA::GFP::let-858 3′UTR	This paper	N/A
myo-3p::arf-1.2::GFP::let-858 3′UTR	This paper	N/A
myo-3p::arf-3::GFP::let-858 3′UTR	This paper	N/A
sur-5p::xbp-1 s::unc-54 3′UTR	Andrew Dillin lab Taylor and Dillin, 2013	N/A
unc-54p::xbp-1 s::unc-54 3′UTR	Andrew Dillin lab Taylor and Dillin, 2013	N/A

(*Continued on next page*)

Continued

REAGENT or RESOURCE	SOURCE	IDENTIFIER
eIF-2a cDNA	Shin Takagi lab Nukazuka et al., 2008	N/A
eIF-2a cDNA *(s49A)*	Shin Takagi lab Nukazuka et al., 2008	N/A
eIF-2a cDNA *(S49D)*	Shin Takagi lab Nukazuka et al., 2008	N/A
myo-3p::eIF-2a cDNA::FLAG::HA::let-858 3′UTR	This paper	N/A
myo-3p::eIF-2a cDNA (s49A):: FLAG::HA::let-858 3′UTR	This paper	N/A
myo-3p::eIF-2a cDNA (S49D):: FLAG::HA::let-858 3′UTR	This paper	N/A
myo-3p::hsp-4::let-858 3′UTR	This paper	N/A
Software and algorithms		
Fiji (ImageJ)	https://fiji.sc	Ver 1.50i; RRID:SCR_002285
Prism 5	GraphPad	N/A

RESOURCE AVAILABILITY

Lead contact

Further information and requests for resources and reagents should be directed to and will be fulfilled by the Lead Contact, Min Han (mhan@colorado.edu).

Materials availability

All reagents generated in this study will be made available on request.

Data and code availability

- This study did not generate large datasets, but raw data/images are available from the lead contact upon request.
- This paper does not report original codes.
- Any additional information required to reanalyze the data reported in this paper is available from the lead contact upon request

EXPERIMENTAL MODEL AND SUBJECT DETAILS

Nematode stocks were maintained on nematode growth medium (NGM) plates seeded with bacteria (*E. coli* OP50) at 20°C, unless otherwise indicated. Hermaphrodites were used for all experiments. The following strains were used in this study: N2, *acs-4(ok2872), acs-17(ok1562)*, RW1596[*myo-3(st386);stEx30*], KAG420[kagIs4[gfp::*myo-3*, V:12226816], VP303[*rde-1(ne219);kbIs7*], SPC272[*sid-1(qt9);Is(myo-3p::SID-1)*], OH122(*mgIs25*), SJ4005(zcIs4), AGD927(uthIs270), RB1104[*hsp-3(ok1083)*], WB141[*pat-6(st561);zpEx99*], DM5115[*unc-112(st581);raEx16*], NK358[*unc-119(ed4);qyIs43*], SJ4100(*zcIs13*), AGD710(*uthIs235*), TJ375(gpIs1(*hsp-16.2::*GFP)), VC1099[*hsp-4(gk514)*] and RB545[*pek-1(ok275)*]. Strain SPC272 was obtained from Gary Rvukun's lab. KAG420 is a gift from Dr. Kathrin Gieseler. All the other *C. elegans* strains were provided by the Caenorhabditis Genetics Center (CGC), which is funded by NIH Office of Research Infrastructure Programs (P40 OD010440).

METHOD DETAILS

Characterization of paralysis, the uncoordinated phenotype, sarcomere structure and ER stress

Animals with a pumping pharynx that did not respond to head/tail touch were characterized as "paralyzed." Animals that showed no body movement, slow body movement or uncoordinated movement were characterized as "uncoordinated." Lethal animals were excluded from the mobility score. The *acs-4(lf);acs-17(lf)* double mutants or *acs-4(lf/+);acs-17(lf)* control animals grown for 72 hours post-hatch were scored for day-1 adult-onset paralysis. The animals with indicated genotypes grown for 72 hours (day 1 adult), 96h (day 2 adult) or 120h (day 3 adult) post hatch, were scored for mobility. Myosin heavy chain, encoded by *myo-3*, is the core component of sarcomere. MYO-3::GFP in strain RW1596[*myo-3(st386);stEx30*], driven by its own promoter, rescues *myo-3(lf)* defect and it is therefore ideal for indicating sarcomere structure. In addition, MYO-3::GFP knock-in strain KAG420 [kagIs4[gfp::*myo-3*] was also used for analyzing sarcomere structure (Mergoud Dit Lamarche et al., 2018]. As previously described, disorganized myofilaments displaying MYO-3::GFP aggregations were scored as having sarcomere defect (Meissner et al., 2009). The UNC-97::GFP integrated transgene is evenly and strongly expressed in all the body wall muscle cells. As long as one body wall muscle cell displayed no

obvious GFP signal, the corresponding worm was scored as having low UNC-97::GFP signal, which was further quantified by western blotting. Briefly, body wall muscle cells of animals with indicated genotypes/treatments showing induction of GFP were scored as displaying ER stress, compared to the control showing no GFP signal.

RNAi by feeding and injection

Some of the RNAi bacteria strains were obtained from the MRC RNAi library (Source BioScience) and ORF RNAi library (GE Dharmacon), unless otherwise noted. For feeding RNAi experiments, animals were treated with RNAi from hatching for two generations. Specifically, for the second generation of RNAi treatment, *hsp-3*(RNAi)-treated animals were scored for mobility or collected for western blot analysis every day between the third day (72 h, day-1 adult), the fourth day (96 h, day-2 adult) and the fifth day (120 h, day-3 adult) post-hatch. For the RNAi treatment of the other genes, animals were treated for three days post-hatch during the second generation of RNAi before scoring mobility or *hsp-4p::GFP* induction and day-1 adult animals displaying paralysis or the uncoordinated phenotype were collected for western blotting. The HT115 bacteria strain containing the pL4440-Dest vector was used as Mock RNAi control for feeding RNAi treatment.

Strains with *sid-1(qt9);Is(myo-3p::SID-1)* or *rde-1(ne219);kbIs7* genetic backgrounds were used for body-wall muscle-specific and intestine-specific RNAi analysis, respectively (Espelt et al., 2005; Jose et al., 2009; Melo and Ruvkun, 2012). For *nmt-1(muscle-RNAi)*, *arf-1.2(muscle-RNAi)* or *arf-3(muscle-RNAi)* treatment, dsRNAs were generated by using the MEGAscript® T7 Kit (Life Technologies) to reverse transcribe the DNA templates that were PCR amplified from the RNAi bacteria strains. The indicated animals were then injected with the corresponding dsRNA and grown for two generations on the corresponding RNAi plates before analysis as described above.

Construction of transgenes

For establishing the transgene Ex(*acs-4p::acs-4 cDNA::GFP::let-858 3′UTR*), we amplified the *acs-4* native promoter (3kb region upstream of the *acs-4* coding sequence) with primers 5′- AGTCAGTCGACGATAATGCAGGATTGCCTCCCGTTATTAT −3′ (Sal I) and 5′-CGGCGGCGGTCTAGACTGTAAATAACGAAAATTAGAAGAG −3′ (Xba I) and *acs-4* cDNA with primers 5′- GCGTCTAGAATGAAACG GAAAGTTTCGGTATACG-3′ (Xba I) and 5′- GCGTGCGGCCGCTTAATTCTTTTTGAGCTGCTT-3′ (Not I). We then cloned these two fragments into the pBlueScript II SK (+) vector with GFP coding sequence and *let-858* 3′UTR. The *gfp* sequence was PCR amplified from the pPD95.77 vector (Addgene). In order to generate the tissue-specific expression plasmid, the *acs-4* promoter region of the plasmid (*acs-4p::acs-4 cDNA::GFP::let-858 3′UTR*) was replaced with a tissue specific promoter, such as promoters of *col-10*, *rgef-1*, *ges-1*, and *myo-3*. For overexpression of *unc-97*, its genomic DNA was amplified with primers 5′- ATATATGGCGCGCCGTACGGA AGGCGCCAATAGCAC-3′(Asc I) and 5′- ACACACGCTAGCTTATTTTGGTCCAGGACTCATCGA-3′ (Nhe I) and cloned into the pBlueScript II SK (+) vector.

To build plasmids (*myo-3p::ARF-1.2::GFP::let-858 3′UTR*) and (*myo-3p::ARF-3::GFP::let-858 3′UTR*), primers 5′-GCGCTTAATTAA TGGGAAACGTGTTCGGCA-GCTTATTT-3′ and 5′-GACTGTCGACAGATCTATTCTTGAGCTGGTTGCTGAG-3′ were used to amplify *arf-1.2* coding sequence and primers 5′- GCGCTTAATTAATGGGTTTA-ACAATCTCCTCCCTCTTC-3′ and 5′- ATATGTCGACGGTCT TGGAAAGCTGGTTGGA-TA GCCAG-3′ were used to obtain *arf-3* genomic coding sequence. These two fragments were then cloned into plasmid (*myo-3p::acs-4 cDNA::GFP::let-858 3′UTR*) to generate vectors (*myo-3p::ARF-1.2::GFP::let-858 3′UTR*) and (*myo-3p::ARF-3::GFP::let-858 3′UTR*) by replacing the *acs-4* cDNA region.

To generate a single copy ARF-1.2::GFP transgene expressing specifically in muscle, the DNA fragment carrying *myo-3p::ARF-1.2::GFP::let-858* was inserted into Chromosome II as a single copy insertion using the CRISPR/Cas9 method (Dickinson and Goldstein, 2016; Dickinson et al., 2013). The GFP expression from this single-copy transgene was similar to that from the multi-copy transgene.

The *sur-5* promoter (*sur-5p*) drives ubiquitous expression in *C. elegans* (Shen et al., 2001; Taylor and Dillin, 2013; Yochem et al., 1998). Plasmids (*sur-5p::xbp-1 s::unc-54 3′UTR*) and (*unc-54p::xbp-1 s::unc-54 3′UTR*) were obtained from Andrew Dillin's lab. The eIF-2a cDNA, eIF-2a(S49A) cDNA, and eIF-2a(S49D) cDNA were obtained from Shin Takagi's lab and primers 5′- GCGCTTAATTAAT GAAATGCCGTTTCTACGAGAATCAATTCCCCGATGTCGAGGAGACCGTTGTCGCCAATGTTAAAATGATTG-3′ and 5′-GGTTGCTA GCTTAAGCGTAATCTGGAACATCGTATGGGTACTTGTCGTCATCGTCTTTGTAGTCATCATCCTCCTCATCACTGT-3′ were used to add FLAG and HA tag. The FLAG- and HA-tagged eIF-2a cDNA, eIF-2a(S49A) cDNA, and eIF-2a(S49D) cDNA fragments were cloned into plasmid (*myo-3p::acs-4 cDNA::GFP::let-858 3′UTR*) to generate plasmids (*myo-3p::eIF-2a cDNA::FLAG::HA::let-858 3′UTR*), (*myo-3p::eIF-2a cDNA(S49A)::FLAG::HA::let-858 3′UTR*) and (*myo-3p::eI-F2a cDNA(S49D)::FLAG::HA::let-858 3′UTR*) by replacing region containing *acs-4* cDNA::GFP.

To make the body-wall muscle-expressed *hsp-4* plasmid, we amplified the *hsp-4* genomic coding sequence by using primers 5′-GCGCGCGCTTAATTAATGAAAGTTTTCTCGTTGATTTTGA-3′ and 5′- AAGCAAGCTAGCTTACAGTTCATCATGATCCTCCGAT-3′. The obtained fragment was sub-cloned into plasmid (*myo-3p::acs-4 cDNA::GFP::let-858 3′UTR*) to generate vector (*myo-3p::HSP-4::let-858 3′UTR*) by replacing *acs-4 cDNA::GFP* region. These obtained plasmids were injected into the germline to create the corresponding extra-chromosomal array transgenes (Evans, 2006).

Analysis of larval lethality

L1-staged *acs-4(lf/+);acs-17(lf)* mutants were grown on plates, with *atf-6(RNAi)* or mock RNAi treatments, to adult stage and 20 of these gravid adults were picked to new plates with corresponding RNAi bacteria. After laying eggs for 3 hours, the mothers were

removed and the eggs were allowed to hatch and grow for another 72 hours before scoring the lethality. To study the phenotype of *acs-4(lf);acs-17(lf);pek-1(lf)* in larval growth, we first picked 20-30 gravid *acs-4(lf/+);acs-17(lf);pek-1(lf)* adults and allowed them to lay eggs for 3 hours. After growing for 72 hours, the *acs-4(lf);acs-17(lf)* progeny were scored for the larval lethality phenotype. Lethality was characterized by lack of movement when touched and lack of pharyngeal pumping.

Western blotting

Worm samples were collected at the same stage and rinsed three times in M9 buffer. After blocking, the corresponding primary antibody [anti-GFP (Clotech, JL-8), anti-PAT-4 (a rabbit polyclonal antibody) (Qadota et al., 2012), anti-PAT-6 (a rat polyclonal antibody) (Warner et al., 2013), anti-FLAG (Sigma, #F3165), anti-Histone H3 (abcam, #ab1791) and anti-p-eIF2alpha (CST, #9721)] and secondary antibody were added for detection. The anti-PAT-4 and anti-PAT-6 antibodies were gifts from Dr. Guy Benian. At least two replicates were analyzed. ImageJ software was used to measure the signal of the bands from the blotting.

Immunostaining

1-day adult *acs-4(lf);acs-17(lf) and acs-4(lf/+);acs-17(lf)* animals were collected and rinsed three times in M9 buffer before dissecting. The dissected worms were immediately incubated in fixation solution [3% formaldehyde, 6 mM K2HPO4 (pH 7.2) and 75% methanol] for 1-3 hours at −20°C. Fixation solution was removed and the sample was rinsed with PBS containing 0.1% Tween-20. Then, incubate the worms in PBS containing 0.1% Tween-20 and 0.5% BSA for 1 hour before adding Alexa Fluor® 546 phalloidin (ThermoFisher, #A22283) at 1:20 dilution. After incubation for 1 hour at room temperature (protected from light), the worms were rinsed with PBS containing 0.1% Tween-20 and 0.5% BSA for 3 times before scoring under the Normarski microscope.

Analysis of myristoylated proteins

Wild-type worms were synchronized at L1 stage and grown on food for 24 hours before transfer to a liquid culture containing S-medium, OP50 food, and either ethanol or 60 μM myristic acid alkyne (Cayman Chemical). After growing in this liquid for another 36 hours, around 600,000 animals of each treatment at early-mid L4 stage were collected, rinsed and sonicated before adding lysis buffer (50 mM HCL-Tris pH 8.0, 0.5% SDS, 0.5% CHAPS, 150 mM NaCl and protease inhibitor). The worms were vortexed in the lysis buffer for 30 minutes at 4°C and then centrifuged at 16,000 g for 5 minutes. The supernatant was transferred to a new tube for the subsequent Click Chemistry reaction [Click reaction kit (#1001, Click Chemistry Tools), azide agarose beads (#1038-2, Click Chemistry Tools). The Click reaction was executed by adding the reducing agent, Cu-chelating agent and Copper Sulfate to the worm lysate. The reaction was protected from light and allowed to incubate overnight at room temperature. The myristoylated proteins were covalently linked with the beads after the reaction. The beads were rinsed rigorously first with wash buffer (100 mM Tris ph = 8.0, 250 mM NaCl and 5 mM EDTA) containing 1% SDS for 5 times and later with wash buffer containing 8M urea for 5 times. Then, the beads were treated with Trypsin to digest the isolated myristoylated proteins from the beads and the resulting peptides were desalted with C-18 resin columns (Pierce, Cat #89870) and lyophilized for mass-spec analysis. The results of the myristoylated protein MS analysis are listed in Table S1.

Analysis of ARF-1.2 and ARF-3 myristoylation

acs-4(lf/+);acs-17(lf) and *acs-4(lf);acs-17(lf)* with transgene Ex(*myo-3p::ARF-1.2::GFP::let-858 3′UTR*) or Ex(*myo-3p::ARF-3::GFP::let-858 3′UTR*) were treated with myristic acid alkyne or solvent as described above. When reaching adulthood, animals were collected, rinsed and subjected to freeze/thaw 5 times before adding lysis buffer (50 mM HCL-Tris pH 8.0, 0.5% SDS, 0.5% CHAPS, 150 mM NaCl and protease inhibitor). Before the Click reaction, a small fraction of worm lysate was analyzed by anti-GFP antibody to determine the total ARF-1.2::GFP and ARF-3::GFP input amount. The other fraction of worm lysate was subjected to the Click reaction with Dde Azide-agarose resin (#1153, Click Chemistry Tools). After the Click reaction, myristoylated proteins were covalently linked with the agarose resin. After removing non-specifically bound proteins by rigorously washing, the resin was incubated in 2% hydrazine solution to release the myristoylated proteins. Western blotting was then used to determine the abundance of myristoylated ARF-1.2::GFP and myristoylated ARF-3::GFP with an anti-GFP antibody (Clotech, JL-8) by running the released proteins on SDS-PAGE.

QUANTIFICATION AND STATISTICAL ANALYSIS

ImageJ software was used to quantify bands from western blots and fluorescence intensity of GFP expression.

For sarcomere gene reporters, number of worms showed organized or disrupted structure was quantified.

To reduce bias, treatments and genotypes were blinded before sample analysis. To randomize the analyzed samples, samples were prepared under a dissection microscope before scoring them with a compound microscope.

All the analyses of statistical significances were calculated by a Student's t test. The data were considered to be significant when $p < 0.05$. The mean ± SD, the exact value and definition of "n" numbers are reported in figures or figure legends. "n" number is defined by number of animals analyzed.